

# Speciated atmospheric mercury and sea-air exchange of gaseous mercury in the South China Sea

Chunjie Wang<sup>1</sup>, Zhangwei Wang<sup>1</sup>, Fan Hui<sup>2</sup>, Xiaoshan Zhang<sup>1</sup>

<sup>1</sup>Research Center for Eco-Environmental Sciences, Chinese Academy of Sciences, 18 Shuangqing Road, Beijing, China

<sup>2</sup>China University of Petroleum (Beijing), 18 Fuxue Road, Beijing, China

Correspondence to: Xiaoshan Zhang (zhangxsh@rcees.ac.cn)

## Abstract

The characteristics of the reactive gaseous mercury (RGM) and particulate mercury ( $\text{Hg}^{\text{P}}$ ) in the marine boundary layer (MBL) is poorly understood due in part to sparse data from sea and ocean. Gaseous elemental Hg (GEM), RGM and size-fractionated  $\text{Hg}^{\text{P}}$  in marine atmosphere, and dissolved gaseous Hg (DGM) in surface seawater were determined in the South China Sea (SCS) during an oceanographic expedition (3–28 September 2015). The mean concentrations of GEM, RGM and  $\text{Hg}^{\text{P}}_{2.5}$  were  $1.52 \pm 0.32 \text{ ng m}^{-3}$ ,  $6.1 \pm 5.8 \text{ pg m}^{-3}$  and  $3.2 \pm 1.8 \text{ pg m}^{-3}$ , respectively. Low GEM level indicated that the SCS suffered less influence from fresh emissions, which could be due to the majority of air masses coming from the open oceans as modeled by backward trajectories. Atmospheric reactive Hg ( $\text{RGM} + \text{Hg}^{\text{P}}_{2.5}$ ) represented less than 1 % of total atmospheric Hg, indicating that atmospheric Hg existed mainly as GEM in the MBL. The GEM and RGM concentrations in the northern SCS ( $1.73 \pm 0.40 \text{ ng m}^{-3}$  and  $7.1 \pm 1.4 \text{ pg m}^{-3}$  respectively) were significantly higher than those in the western SCS ( $1.41 \pm 0.26 \text{ ng m}^{-3}$  and  $3.8 \pm 0.7 \text{ pg m}^{-3}$ ), and the  $\text{Hg}^{\text{P}}_{2.5}$  and  $\text{Hg}^{\text{P}}_{10}$  levels ( $8.3$  and  $24.4 \text{ pg m}^{-3}$ ) in the Pearl River Estuary (PRE) were 0.5–6.0 times higher than those in the open waters of the SCS, suggesting that the PRE was polluted to some extent. The size distribution of  $\text{Hg}^{\text{P}}$  in  $\text{PM}_{10}$  was observed to be three-modal with peaks around  $<0.4$ ,  $0.7$ – $1.1$  and  $5.8$ – $9.0 \text{ }\mu\text{m}$ , respectively, but the coarse modal was the dominant size, especially in the open SCS. There was no significant diurnal pattern of GEM and  $\text{Hg}^{\text{P}}_{2.5}$ , but we found the mean RGM concentration was significantly higher in daytime ( $8.0 \pm 5.5 \text{ pg m}^{-3}$ ) than in nighttime ( $2.2 \pm 2.7 \text{ pg m}^{-3}$ ) mainly due to the influence of solar radiation. In the northern SCS, the DGM concentrations in nearshore area ( $40$ – $55 \text{ pg l}^{-1}$ ) were about twice as high as those in the open sea, but this pattern was not significant in the western SCS. The sea-air exchange fluxes of  $\text{Hg}^0$  in the SCS varied from  $0.40$  to  $12.71 \text{ ng m}^{-2} \text{ h}^{-1}$  with a mean value of  $4.99 \pm 3.32 \text{ ng m}^{-2} \text{ h}^{-1}$ . The annual emission flux of  $\text{Hg}^0$  from the SCS to the atmosphere was estimated to be  $159.6 \text{ tons yr}^{-1}$ , accounting for about 5.54 % of the global  $\text{Hg}^0$  oceanic evasion although the SCS only represents 1.0 % of the global ocean area. Additionally, the annual dry deposition flux of atmospheric reactive Hg represented more than 18 % of the annual evasion flux of  $\text{Hg}^0$ , and

35 therefore the dry deposition of atmospheric reactive Hg was an important pathway for the input of  
36 atmospheric Hg to the SCS.

## 37 **1 Introduction**

38 Mercury (Hg) is a naturally occurring metal, and it is generally released to the environment  
39 through both the natural and anthropogenic pathways (Schroeder and Munthe, 1998). However,  
40 since the Industrial Revolution, the anthropogenic emissions of Hg increased drastically.  
41 Continued rapid industrialization has made Asia the largest source region of Hg emissions to air,  
42 with East and Southeast Asia accounting for about 40 % of the global total (UNEP, 2013). Three  
43 operationally defined Hg forms are present in the atmosphere: gaseous elemental Hg (GEM or  
44  $\text{Hg}^0$ ), reactive gaseous Hg (RGM) and particulate Hg ( $\text{Hg}^P$ ) (Schroeder and Munthe, 1998; Landis  
45 et al., 2002), while they have different physicochemical characteristics. GEM is very stable with a  
46 residence time of 0.2–1.0 yr due to its high volatility and low solubility (Radke et al., 2007; Selin  
47 et al., 2007; Horowitz et al., 2017). Therefore, GEM can be transported for a long-range distance  
48 in the atmosphere, and this makes it well-mixed on a regional and global scale. Generally, GEM  
49 makes up more than 95 % of total atmospheric Hg (TAM), while the RGM and  $\text{Hg}^P$  concentrations  
50 (collectively known as atmospheric reactive mercury) are typically 2–3 orders of magnitude  
51 smaller than GEM in part because they are easily removed from ambient air by wet and dry  
52 deposition (Laurier and Mason, 2007; Holmes et al., 2009; Gustin et al., 2013), and they can also  
53 be reduced back to  $\text{Hg}^0$ . It should be noted that all of the acronyms in this article have been listed  
54 in the Appendix.

55 Numerous previous studies have shown that  $\text{Hg}^0$  in the marine boundary layer (MBL) can be  
56 rapidly oxidized to form RGM in situ (Laurier et al., 2003; Sprovieri et al., 2003, 2010; Laurier  
57 and Mason, 2007; Soerensen et al., 2010a; Wang et al., 2015; Mao et al., 2016; Ye et al., 2016).  
58 Ozone and OH could potentially be important oxidants on aerosols (Ariya et al., 2015; Ye et al.,  
59 2016), while the reactive halogen species (e.g., Br, Cl and BrO, generating from sea salt aerosols)  
60 may be the dominant sources for the oxidation of  $\text{Hg}^0$  in the MBL (Holmes et al., 2006, 2010;  
61 Auzmendi-Murua et al., 2014; Gratz et al., 2015; Steffen et al., 2015; Shah et al., 2016; Horowitz  
62 et al., 2017). However, a recent study showed that Br and BrO became dominant GEM oxidants in  
63 the marine atmosphere with mixing ratios reaching 0.1 and 1 pptv, respectively, and contributing ~  
64 70 % of the total RGM production during midday, while  $\text{O}_3$  dominated GEM oxidation (50–90 %  
65 of RGM production) when Br and BrO mixing ratios were diminished (Ye et al., 2016). The wet  
66 and dry deposition (direct or uptake by sea-salt aerosol) represents a major input of RGM and  $\text{Hg}^P$   
67 to the sea and ocean due to their special and unique characteristics (i.e., high reactivity and water  
68 solubility) (Landis et al., 2002; Holmes et al., 2009). Previous studies also showed that  
69 atmospheric wet and dry deposition of RGM (mainly  $\text{HgBr}_2$ ,  $\text{HgCl}_2$ ,  $\text{HgO}$ , Hg-nitrogen and sulfur  
70 compounds) was the greatest source of Hg to open oceans (Holmes et al., 2009; Mason et al., 2012;

71 Huang et al., 2017). A recent study suggested that approximately 80 % of atmospheric reactive Hg  
72 sinks into the global oceans, and most of the deposition takes place to the tropical oceans  
73 (Horowitz et al., 2017).

74 The atmospheric reactive Hg deposited to the oceans follows different reaction pathways.  
75 One important process is that divalent Hg can be combined with the existing particles followed by  
76 sedimentation, or be converted to methylmercury (MeHg), the most bioaccumulative and toxic  
77 form of Hg in seafood (Ahn et al., 2010; Mason et al., 2017). Another important process is that the  
78 divalent Hg can be converted to dissolved gaseous Hg (DGM) through abiotic and biotic  
79 mechanisms (Strode et al., 2007). It is well known that almost all DGM in the surface seawater is  
80  $\text{Hg}^0$  (Horvat et al., 2003), while the dimethylmercury is extremely rare in the surface seawater  
81 (Bowman et al., 2015). It has been found that a majority of the surface seawater was  
82 supersaturated with respect to  $\text{Hg}^0$  (Soerensen et al., 2010b, 2013, 2014), and parts of this  $\text{Hg}^0$   
83 may be emitted to the atmosphere. Evasion of  $\text{Hg}^0$  from the oceanic surface into the atmosphere is  
84 partly driven by the solar radiation and aquatic Hg pools of natural and anthropogenic origins  
85 (Andersson, et al., 2011). Sea-air exchange is an important component of the global Hg cycle as it  
86 mediates the rate of increase in ocean Hg and therefore the rate of change in level of MeHg.  
87 Consequently,  $\text{Hg}^0$  evasion from sea surface not only decreases the amount of Hg available for  
88 methylation in waters but also has an important effect on the redistribution of Hg in the global  
89 environment (Strode et al., 2007).

90 In recent years, speciated atmospheric Hg has been monitored in coastal areas (Xu et al.,  
91 2015; Ye et al., 2016; Howard et al., 2017; Mao et al., 2017) and open seas and oceans (e.g.,  
92 Chand et al., 2008; Soerensen et al., 2010a; Mao et al., 2016; Wang et al., 2016a, b). However,  
93 there exists a dearth of knowledge regarding speciated atmospheric Hg and sea-air exchange of  
94  $\text{Hg}^0$  in tropical seas, such as the South China Sea (SCS). The highly time-resolved ambient GEM  
95 concentrations were measured using a Tekran<sup>®</sup> system. Simultaneously, the RGM,  $\text{Hg}^{\text{P}}$  and DGM  
96 were measured using manual methods. The main objectives of this study are to identify the  
97 spatial-temporal characteristics of speciated atmospheric Hg and to investigate the DGM  
98 concentrations in the SCS during the cruise in September 2015, and then to calculate the  $\text{Hg}^0$  flux  
99 based on the meteorological parameters as well as the concentrations of GEM in air and DGM in  
100 surface seawater. These results will raise our knowledge of the Hg cycle in tropical marine  
101 atmosphere and waters.

## 102 **2 Materials and methods**

### 103 **2.1 Study area**

104 The SCS is located in the downwind of Southeast Asia (Fig. 1a), and it is the largest semi-enclosed  
105 marginal sea in the western tropical Pacific Ocean. The SCS is connected with the East China Sea  
106 (ECS) to the northeast and the western Pacific Ocean to the east (Fig. 1a). The SCS is surrounded

107 by numerous developing and developed countries (Fig. 1a). An open cruise was organized by the  
108 South China Sea Institute of Oceanology (Chinese Academy of Sciences) and conducted during  
109 the period of 3–28 September 2015. The sampling campaign was conducted on R/V *Shiyan 3*,  
110 which departed from Guangzhou, circumnavigated the northern and western SCS and then  
111 returned to Guangzhou. The DGM sampling stations and R/V tracks were plotted in Fig. 1b. In  
112 this study, meteorological parameters (including photosynthetically available radiation (PAR)  
113 (Li-COR<sup>®</sup>, Model: Li-250), wind speed, air temperature and RH) were measured synchronously  
114 with atmospheric Hg onboard the R/V.

## 115 2.2 Experimental methods

### 116 2.2.1 Atmospheric GEM measurements

117 In this study, GEM was measured using an automatic dual channel, single amalgamation cold  
118 vapor atomic fluorescence analyzer (Model 2537B, Tekran<sup>®</sup>, Inc., Toronto, Canada), which has  
119 been reported in our previous studies (Wang et al., 2016a, b, c). In order to reduce the  
120 contamination from ship exhaust plume as possible, we installed the Tekran<sup>®</sup> system inside the  
121 ship laboratory (the internal air temperature was controlled to 25 °C using an air conditioner) on  
122 the fifth deck of the R/V and mounted the sampling inlet at the front deck 1.5 m above the top  
123 deck (about 16 m above sea level) using a 7 m heated (maintained at 50 °C)  
124 polytetrafluoroethylene (PTFE) tube (¼ inch in outer diameter). The sampling interval was 5 min  
125 and the air flow rate was 1.5 l min<sup>-1</sup> in this study. Moreover, two PTFE filters (0.2 µm pore size,  
126 47 mm diameter) were positioned before and after the heated line, and the soda lime before the  
127 instrument was changed every 3 days during the cruise. The Tekran<sup>®</sup> instrument was calibrated  
128 every 25 h using the internal calibration source and these calibrations were checked by injections  
129 of certain volume of saturated Hg<sup>0</sup> before and after this cruise. The relative percent difference  
130 between manual injections and automated calibrations was < 5 %. The precision of the analyzer  
131 was determined to > 97 %, and the detection limit was < 0.1 ng m<sup>-3</sup>.

132 The meteorological and basic seawater parameters were collected onboard the R/V, which  
133 was equipped with meteorological and oceanographic instrumentations. To investigate the  
134 influence of air masses movements on the GEM levels, 72-h backward trajectories of air masses  
135 were calculated using the Hybrid Single Particle Lagrangian Integrated Trajectory (HYSPLIT)  
136 model (Draxler and Rolph, 2012) and TrajStat software (Wang et al., 2009) based on Geographic  
137 Information System. Global Data Assimilation System (GDAS) meteorological dataset  
138 (<ftp://arlftp.arlhq.noaa.gov/pub/archives/gdas1/>) with 1° × 1° latitude and longitude horizontal  
139 spatial resolution and 23 vertical levels at 6-h intervals was used as the HYSPLIT model input. It  
140 should be noted that the start time of each back trajectory was identical to the GEM sampling time  
141 (UTC) and the start height was set at 500 m above sea level to represent the approximate height of  
142 the mixing MBL where atmospheric pollutants were well mixed.

## 143 2.2.2 Sampling and analysis of RGM and Hg<sup>P</sup>

144 The Hg<sup>P</sup><sub>2.5</sub> (Hg<sup>P</sup> in PM<sub>2.5</sub>) was collected on quartz filter (47 mm in diameter, Whatman), which has  
145 been reported in several previous studies (Landis et al., 2002; Liu et al., 2011; Kim et al., 2012). It  
146 should be pointed out that the KCl coated denuders were heated at 500 °C for 1 h and the quartz  
147 filters were pre-cleaned by pyrolysis at 900 °C for 3 h to remove the possible pollutant. The RGM  
148 and Hg<sup>P</sup><sub>2.5</sub> were sampled using a manual system (URG-3000M), which has been reported in  
149 previous studies (Landis et al., 2002; Liu et al., 2011; Wang et al., 2016b). The sampling unit  
150 includes an insulated box (Fig. S1), two quartz annular denuders, two Teflon filter holder (URG  
151 Corporation) and a pump etc. The sampling flow rate was 10 l min<sup>-1</sup> (Landis et al., 2002), and the  
152 sampling inlet was 1.2 m above the top deck of the R/V. In this study, one Hg<sup>P</sup><sub>2.5</sub> sample was  
153 collected in the daytime (6:00–18:00) and the other in the nighttime (18:00–6:00 (next day)),  
154 while two RGM samples were collected in the daytime (6:00–12:00 and 12:00–18:00, local time)  
155 and one RGM sample in the nighttime. Quality assurance and quality control for Hg<sup>P</sup> and RGM  
156 were carried out using field blank samples and duplicates. The field blank denuders and quartz  
157 filters were treated similarly to the other samples but not sampling. The mean relative differences  
158 of duplicated Hg<sup>P</sup><sub>2.5</sub> and RGM samples (n = 6) were 13 ± 6 % and 9 ± 7 %, respectively.

159 Meanwhile, we collected different size particles using an Andersen impactor (nine-stage),  
160 which has been widely used in previous studies (Feddersen et al., 2012; Kim et al., 2012; Zhu et  
161 al., 2014; Wang et al., 2016a). The Andersen cascade impactor was installed on the front top deck  
162 of the R/V to sample the size-fractionated particles in PM<sub>10</sub>. In order to diminish the contamination  
163 from exhaust plume of the ship as much as possible, we turned off the pump when R/V arrived at  
164 stations, and then switched back on when the R/V went to next station. The sample collection  
165 began in the morning (10:00 am) and continued for 2 days with a sampling flow rate of 28.3 l  
166 min<sup>-1</sup>. Field blanks for Hg<sup>P</sup> were collected by placing nine pre-cleaned quartz filters (81 mm in  
167 diameter, Whatman) in another impactor for 2 days without turning on the pump. After sampling,  
168 the quartz filters were placed in cleaned plastic boxes (sealing in Zip Lock plastic bags), and then  
169 were immediately preserved at -20 °C until the analysis.

170 The detailed analysis processes of RGM and Hg<sup>P</sup> have been reported in our previous studies  
171 (Wang et al., 2016a, b). Briefly, the denuder and quartz filter were thermally desorbed at 500 °C  
172 and 900 °C, respectively, and then the resulting thermally decomposed Hg<sup>0</sup> in carrier gas (zero air,  
173 i.e., Hg-free air) was quantified. The method detection limit was calculated to be 0.67 pg m<sup>-3</sup> for  
174 RGM based on 3 times the standard deviation of the blanks (n = 57) for the whole dataset. The  
175 average field blank value of denuders was 1.2 ± 0.6 pg (n = 6), while the average blank values (n =  
176 6) of Hg<sup>P</sup><sub>2.5</sub> and Hg<sup>P</sup><sub>10</sub> were 1.4 pg (equivalent of < 0.2 pg m<sup>-3</sup> for a 12 h sampling time) and 3.2  
177 pg (equivalent of < 0.04 pg m<sup>-3</sup> for a 2-day sampling time) of Hg per filter, respectively. The  
178 detection limits of Hg<sup>P</sup><sub>2.5</sub> and Hg<sup>P</sup><sub>10</sub> were all less than 1.5 pg m<sup>-3</sup> based on 3 times the standard  
179 deviation of field blanks. It should be noted that all the observed RGM and Hg<sup>P</sup> values were

180 higher than the corresponding blank values, and the average blank values for RGM and Hg<sup>P</sup> were  
181 subtracted from the samples.

### 182 **2.2.3 Determination of DGM in surface seawater**

183 In this study, the analysis was carried out according to the trace element clean technique, all  
184 containers (borosilicate glass bottles and PTFE tubes, joints and valves) were cleaned prior to use  
185 with detergent, followed by trace-metal-grade HNO<sub>3</sub> and HCl, and then rinsed with Milli-Q water  
186 (> 18.2 MΩ cm<sup>-1</sup>), which has been described in our previous study (Wang et al., 2016c). DGM  
187 were measured in situ using a manual method (Fu et al., 2010; Ci et al., 2011). The detailed  
188 sampling and analysis of DGM has been elaborated in our previous study (Wang et al., 2016c).  
189 The analytical blanks were conducted onboard the R/V by extracting Milli-Q water for DGM. The  
190 mean concentration of DGM blank was 2.3 ± 1.2 pg l<sup>-1</sup> (n = 6), accounting for 3–10 % of the raw  
191 DGM in seawater samples. The method detection limit was 3.6 pg l<sup>-1</sup> on the basis of three times  
192 the standard deviation of system blanks. The relative standard deviation of duplicate samples  
193 generally < 8 % of the mean concentration (n = 6).

### 194 **2.2.4 Estimation of sea-air exchange flux of Hg<sup>0</sup>**

195 The sea-air flux of Hg<sup>0</sup> was calculated using a thin film gas exchange model developed by Liss  
196 and Slater (1974) and Wanninkhof (1992). The detailed calculation processes of Hg<sup>0</sup> flux have  
197 been reported in recent studies (Ci et al., 2011; Kuss, 2014; Wang et al., 2016c; Kuss et al., 2018).  
198 It should be noted that the Schmidt number for gaseous Hg ( $Sc_{Hg}$ ) is defined as the following  
199 equation:  $Sc_{Hg} = \nu/D_{Hg}$ , where  $\nu$  is the kinematic viscosity (cm<sup>2</sup> s<sup>-1</sup>) of seawater calculated using  
200 the method of Wanninkhof (1992),  $D_{Hg}$  is the Hg<sup>0</sup> diffusion coefficient (cm<sup>2</sup> s<sup>-1</sup>) in seawater,  
201 which is calculated according to the recent research (Kuss, 2014). The degree of Hg<sup>0</sup> saturation ( $S_a$ )  
202 was calculated using the following equation:  $S_a = H' DGM_{conc.}/GEM_{conc.}$ , and the calculation of  $H'$   
203 (the dimensionless Henry's Law constant) has been reported in previous studies (Ci et al., 2011,  
204 2015; Kuss, 2014).

## 205 **3 Results and discussion**

### 206 **3.1 Speciated atmospheric Hg concentrations**

207 Figure 2 shows the time series of speciated atmospheric Hg and meteorological parameters during  
208 the cruise in the SCS. The GEM concentration during the whole study period ranged from 0.92 to  
209 4.12 ng m<sup>-3</sup> with a mean value of 1.52 ± 0.32 ng m<sup>-3</sup> (n = 4673), which was comparable to the  
210 average GEM levels over the global oceans (1.4–1.6 ng m<sup>-3</sup>, Soerensen et al., 2010a, 2013) and  
211 Atlantic Ocean (1.63 ± 0.02 ng m<sup>-3</sup>, Laurier and Mason, 2007), and higher than those at  
212 background sites in the Southern Hemisphere (0.85–1.05 ng m<sup>-3</sup>, Slemr et al., 2015; Howard et  
213 al., 2017), and also higher than those in remote oceans, such as the Cape Verde Observatory

214 station ( $1.19 \pm 0.13 \text{ ng m}^{-3}$ , Read et al., 2017), equatorial Pacific Ocean ( $1.15\text{--}1.05 \text{ ng m}^{-3}$ ,  
215 Soerensen et al., 2014) and Indian Ocean ( $1.0\text{--}1.2 \text{ ng m}^{-3}$ , Witt et al., 2010; Angot et al., 2014),  
216 but lower than those in marginal seas, such as the Bohai Sea (BS), Yellow Sea (YS) and ECS  
217 (Table 1). However, previous studies conducted in the northern SCS showed that the average  
218 GEM concentrations in their study period ( $2.6\text{--}3.5 \text{ ng m}^{-3}$ , Fu et al., 2010; Tseng et al., 2012)  
219 were higher than that in this study. This is due to the fact that the GEM level in the northern SCS  
220 (Fu et al., 2010; Tseng et al., 2012) were considerably higher than that in the western SCS (this  
221 study).

222 The  $\text{Hg}^{\text{P}}_{2.5}$  concentrations over the SCS ranged from 1.2 to  $8.3 \text{ pg m}^{-3}$  with a mean value of  
223  $3.2 \pm 1.8 \text{ pg m}^{-3}$  ( $n = 39$ ) (Fig. 2), which was higher than those observed at Nam Co (China) and  
224 the Amsterdam Island, and were comparable to those in other coastal areas, such as the Okinawa  
225 Island, Nova Scotia, Adriatic Sea, Ontario lake and Weeks Bay (see Table 1), but lower than those  
226 in the BS and YS (Wang et al., 2016b), and considerably lower than those in rural and urban sites,  
227 such as Xiamen, Seoul (see Table 1), Guiyang and Waliguan (Fu et al., 2011, 2012). The results  
228 showed that the SCS suffered less influence from fresh emissions. The RGM concentration over  
229 the SCS ranged from 0.27 to  $27.57 \text{ pg m}^{-3}$  with a mean value of  $6.1 \pm 5.8 \text{ pg m}^{-3}$  ( $n = 58$ ), which  
230 was comparable to those in other seas, such as the North Pacific Ocean, North Atlantic Ocean and  
231 Mediterranean Sea (including the Adriatic Sea) (Table 1), and higher than the global mean RGM  
232 concentration in the MBL (Soerensen et al., 2010a), and also higher than those measured at a few  
233 rural sites (Valente et al., 2007; Liu et al., 2010; Cheng et al., 2013, 2014), but significantly much  
234 lower than those polluted urban areas in China and South Korea, such as Guiyang ( $35.7 \pm 43.9 \text{ pg}$   
235  $\text{m}^{-3}$ , Fu et al., 2011), Xiamen, and Seoul (Table 1). Furthermore, Figure 2 shows that the  
236 long-lived GEM has smaller variability compared to the short-lived species like RGM and  $\text{Hg}^{\text{P}}_{2.5}$ ,  
237 indicating that atmospheric reactive Hg was easily scavenged from the marine atmosphere due not  
238 only to their characteristics (high activity and solubility) but also due to their sensitivity to  
239 meteorological conditions and chemical environments. This pattern was consistent with our  
240 previous observed patterns in the BS and YS (Wang et al., 2016b). Moreover, we found that  
241 atmospheric reactive Hg represents less than 1 % of TAM in the atmosphere, which was  
242 comparable to those measured in other marginal and inner seas, such as the BS and YS (Wang et  
243 al., 2016b), Adriatic Sea (Sprovieri and Pirrone, 2008), Okinawa Island (located in the ECS)  
244 (Chand et al., 2008), but was significantly lower than those at the urban sites (Table 1).

## 245 **3.2 Spatial distribution of atmospheric Hg**

### 246 **3.2.1 Spatial distributions of GEM and RGM**

247 The spatial distribution of GEM over the SCS was illustrated in Fig. 3a. The mean GEM  
248 concentration in the northern SCS ( $1.73 \pm 0.40 \text{ ng m}^{-3}$  with a range of  $1.01\text{--}4.12 \text{ ng m}^{-3}$ ) was  
249 significantly higher than that in the western SCS ( $1.41 \pm 0.26 \text{ ng m}^{-3}$  with a range of  $0.92\text{--}2.83 \text{ ng}$

250  $\text{m}^{-3}$ ) ( $t$ -test,  $p < 0.01$ ). Additionally, we found that the GEM concentrations in the PRE (the  
251 average value  $> 2.00 \text{ ng m}^{-3}$ ) were significantly higher than those in the open SCS (see Figs. 2 and  
252 3a), indicating that this nearshore area suffered from high GEM pollution in our study period  
253 probably due to the surrounding human activities. Figure 3a showed that there was large  
254 difference in GEM concentration between stations 1–10 and stations 16–31. The 72-h  
255 back-trajectories of air masses showed that the air masses with low GEM levels between stations 1  
256 and 10 mainly originated from the SCS (Fig. S2a), while the air masses with high GEM levels at  
257 stations 16–31 primarily originated from East China and ECS, and then passed over the southeast  
258 coastal regions of China (Fig. S2b). Additionally, it could be found that there was small variability  
259 of GEM concentrations over the western SCS except the measurements near the station 79 (Fig.  
260 3a). The back-trajectories showed that the air masses with elevated GEM level near the station 79  
261 originated from the south of the Taiwan Island, while the other air masses mainly originated from  
262 the West Pacific Ocean (Fig. S3a) and the Andaman Sea (Fig. S3b). Therefore, the air masses  
263 dominantly originated from sea and ocean in this study period, and this could be the main reason  
264 for the low GEM level over the SCS. In conclusion, GEM concentrations showed a conspicuous  
265 dependence on the sources and movement patterns of air masses during this cruise.

266 The spatial distribution of RGM over the SCS was plotted in Fig. 3b. The mean RGM  
267 concentration in the northern SCS ( $7.1 \pm 1.4 \text{ pg m}^{-3}$ ) was also obviously higher than that in the  
268 western SCS ( $3.8 \pm 0.7 \text{ pg m}^{-3}$ ) ( $t$ -test,  $p < 0.05$ ), indicating that a portion of RGM in the northern  
269 SCS maybe originated from the anthropogenic emission. We observed elevated RGM  
270 concentrations in the PRE, and this spatial distribution pattern was consistent with that of GEM,  
271 indicating that part of the RGM near PRE probably originated from the surrounding human  
272 activities. This is confirmed by the following fact: The RGM concentrations in nighttime of the  
273 two days in the PRE were  $11.3$  and  $5.2 \text{ pg m}^{-3}$  (Figs. 3b and S4), and they were significantly  
274 higher than those in the open SCS. Another obvious feature was that the amplitude of RGM  
275 concentration was much greater than the GEM, and this further indicated that the RGM was easily  
276 removed from the atmosphere through both the wet and dry deposition. In addition, we found that  
277 the RGM concentrations in the nearshore area were not always higher than those in the open sea  
278 except the measurements in the PRE, suggesting that the RGM in the remote marine atmosphere  
279 presumably not originated from land but from the in situ photo-oxidation of  $\text{Hg}^0$ , which had been  
280 reported in previous studies (e.g., Hedgecock and Pirrone, 2001; Lindberg et al., 2002; Laurier et  
281 al., 2003; Sprovieri et al., 2003, 2010; Sheu and Mason, 2004; Laurier and Mason, 2007;  
282 Soerensen et al., 2010a; Wang et al., 2015).

### 283 **3.2.2 Spatial distributions of $\text{Hg}_{2.5}^{\text{P}}$ and $\text{Hg}_{10}^{\text{P}}$**

284 The concentrations and spatial distribution of  $\text{Hg}_{2.5}^{\text{P}}$  in the MBL were illustrated in Fig. 4a. The  
285 highest  $\text{Hg}_{2.5}^{\text{P}}$  value ( $8.3 \text{ pg m}^{-3}$ ) was observed in the PRE during daytime on 4 September 2015



286 presumably due to the local human activities. The homogeneous distribution and lower level of  
287  $\text{Hg}^{\text{P}}_{2.5}$  in the open SCS indicated that the  $\text{Hg}^{\text{P}}_{2.5}$  not originated from the land and the SCS suffered  
288 less influence from human activities especially in the open sea. This is due to the fact that the  
289 majority of air masses in the SCS during this study period came from the seas and oceans. The  
290 spatial distribution pattern of  $\text{Hg}^{\text{P}}_{2.5}$  in this study was different from our previous observed  
291 patterns in the BS and YS (Wang et al., 2016b), which showed that  $\text{Hg}^{\text{P}}_{2.5}$  concentrations in  
292 nearshore area were higher than those in the open sea both in spring and fall mainly due to the  
293 outflow of atmospheric  $\text{Hg}^{\text{P}}$  from East China.

294 The concentrations and spatial distributions of  $\text{Hg}^{\text{P}}_{10}$  in the MBL of the SCS were illustrated  
295 in Fig. 4b. We found that the  $\text{Hg}^{\text{P}}_{10}$  concentration was considerably (1–6 times) higher in the PRE  
296 than those of other regions of the SCS probably due to the large emissions of anthropogenic Hg in  
297 surrounding areas of the PRE. Moreover, the highest  $\text{Hg}^{\text{P}}_{2.1}/\text{Hg}^{\text{P}}_{10}$  ratio (41 %) was observed in the  
298 PRE and coastal sea area of Hainan Island, while lowest ratio (22 %) was observed in the open sea  
299 (Fig. 4b). The  $\text{Hg}^{\text{P}}_{10}$  concentrations and  $\text{Hg}^{\text{P}}_{2.1}/\text{Hg}^{\text{P}}_{10}$  ratios were higher in the nearshore area  
300 compared to those in the open sea, demonstrating that coastal sea areas are polluted by  
301 anthropogenic Hg to a certain extent. Interestingly, we found the mean  $\text{Hg}^{\text{P}}_{2.1}$  concentration ( $3.16$   
302  $\pm 2.69 \text{ pg m}^{-3}$ ,  $n = 10$ ) measured using the Andersen sampler was comparable to the mean  $\text{Hg}^{\text{P}}_{2.5}$   
303 concentration ( $3.33 \pm 1.89 \text{ pg m}^{-3}$ ,  $n = 39$ ) measured using a 47 mm Teflon filter holder ( $t$ -test,  $p >$   
304  $0.1$ ). This indicated that the fine  $\text{Hg}^{\text{P}}$  level in the MBL of the SCS was indeed low, and there might  
305 be no significant difference in  $\text{Hg}^{\text{P}}$  concentration in the SCS between 12 h and 48 h sampling time.

306 The concentrations of all size-fractionated  $\text{Hg}^{\text{P}}$  were summarized in Table S1. The size  
307 distribution of  $\text{Hg}^{\text{P}}$  in the MBL of the SCS was plotted in Fig. 5. One striking feature was that the  
308 three-modal pattern with peaks around  $<0.4$ ,  $0.7$ – $1.1$  and  $5.8$ – $9.0 \mu\text{m}$  was observed for the size  
309 distributions of  $\text{Hg}^{\text{P}}$  in the open sea (Fig. 5a) if we excluded the data in the PRE. The three-modal  
310 pattern was more obvious when we consider all the data (Fig. 5b). Generally, the  $\text{Hg}^{\text{P}}$   
311 concentrations in coarse particles were significantly higher than those in fine particles, and  $\text{Hg}^{\text{P}}_{2.1}$   
312 contributed approximately 32 % (22–41 %, see Fig. 4b) to the  $\text{Hg}^{\text{P}}_{10}$  for the whole data, indicating  
313 that the coarse mode was the dominant size during this study period. This might be explained by  
314 the sources of the air masses. Since air masses dominantly originated from sea and ocean (Figs. S1,  
315 S2) and contained high concentrations of sea salts which generally exist in the coarse mode ( $1$ – $10$   
316  $\mu\text{m}$ ) (Athanasopoulou et al., 2008; Mamane et al., 2008), the  $\text{Hg}^{\text{P}}_{2.1}/\text{Hg}^{\text{P}}_{10}$  ratios were generally  
317 lower in the SCS compared to those in the BS, YS and ECS (Wang et al., 2016a).

### 318 3.3 Dry deposition fluxes of RGM and $\text{Hg}^{\text{P}}$

319 The dry deposition flux of  $\text{Hg}^{\text{P}}_{10}$  was obtained by summing the dry deposition fluxes of each  
320 size-fractionated  $\text{Hg}^{\text{P}}$  in the same set. The dry deposition flux of  $\text{Hg}^{\text{P}}_{10}$  is calculated using the  
321 following equation:  $F = \sum \text{CHg}^{\text{P}} \times V_d$ , the  $F$  is the dry deposition flux of  $\text{Hg}^{\text{P}}_{10}$  ( $\text{ng m}^{-2} \text{d}^{-1}$ ),  $\text{CHg}^{\text{P}}$

322 is the concentration of  $\text{Hg}^{\text{P}}$  in each size fraction ( $\text{pg m}^{-3}$ ), and  $V_{\text{d}}$  is the corresponding dry  
323 deposition velocity ( $\text{cm s}^{-1}$ ). In this study, the dry deposition velocities of 0.03, 0.01, 0.06, 0.15  
324 and  $0.55 \text{ cm s}^{-1}$  (Giorgi, 1988; Pryor et al., 2000; Nho-Kim et al., 2004) were chosen for the  
325 following size-fractionated particles:  $< 0.4$ ,  $0.4\text{--}1.1$ ,  $1.1\text{--}2.1$ ,  $2.1\text{--}5.8$  and  $5.8\text{--}10 \mu\text{m}$ , respectively  
326 (Wang et al., 2016a). The average dry deposition flux of  $\text{Hg}^{\text{P}}_{10}$  was estimated to be  $1.08 \text{ ng m}^{-2} \text{ d}^{-1}$   
327 based on the average concentration of each size-fractionated  $\text{Hg}^{\text{P}}$  in the SCS (Table S2), which  
328 was lower than those in the BS, YS and ECS (Wang et al., 2016a). The dry deposition velocity of  
329 RGM was  $4.0\text{--}7.6 \text{ cm s}^{-1}$  because of its characteristics and rapid uptake by sea salt aerosols  
330 followed by deposition (Poissant et al., 2004; Selin et al., 2007). The annual dry deposition fluxes  
331 of  $\text{Hg}^{\text{P}}_{10}$  and RGM to the SCS were calculated to be 1.42 and  $27.39\text{--}52.05 \text{ tons yr}^{-1}$  based on the  
332 average  $\text{Hg}^{\text{P}}_{10}$  and RGM concentrations and the area of the SCS ( $3.56 \times 10^{12} \text{ m}^2$ ). The result  
333 showed that RGM contributed more than 95 % to the total dry deposition of atmospheric reactive  
334 Hg. The annual dry deposition flux of RGM was considerably higher than that of the  $\text{Hg}^{\text{P}}_{10}$  due to  
335 the higher deposition rate and concentration of RGM in the SCS.

### 336 **3.4 Temporal variation of atmospheric Hg**

#### 337 **3.4.1 diurnal variation of GEM**

338 The diurnal variation of GEM concentration during the whole study period was illustrated in Fig.  
339 6. It was notable that there was no significant variability of the mean ( $\pm$  SD) GEM concentration  
340 in a whole day during this study period, and the GEM concentration dominantly fell in the range  
341 of  $1.3\text{--}1.7 \text{ ng m}^{-3}$  (Fig. 6). The statistical result showed that the mean GEM concentration in the  
342 daytime (6:00–18:00) ( $1.49 \pm 0.06 \text{ pg m}^{-3}$ ) was comparable to that in the nighttime ( $1.51 \pm 0.06$   
343  $\text{pg m}^{-3}$ ) (*t*-test,  $p > 0.05$ ). The lower GEM concentrations and smaller variability over the SCS  
344 further revealed that the SCS suffered less influence of fresh emissions.

#### 345 **3.4.2 Daily variation of RGM**

346 The average RGM concentrations in the daytime and nighttime were illustrated in Fig. 7. Firstly, it  
347 could be found that RGM showed a diurnal variation with higher concentrations in the daytime  
348 and lower concentrations in the nighttime during the whole study period. The mean RGM  
349 concentration in the daytime ( $8.0 \pm 5.5 \text{ pg m}^{-3}$ ) was significantly and considerably higher than that  
350 in the nighttime ( $2.2 \pm 2.7 \text{ pg m}^{-3}$ ) (*t*-test,  $p < 0.001$ ). This diurnal pattern was in line with the  
351 previous studies (Laurier and Mason, 2007; Liu et al., 2007; Engle et al., 2008; Cheng et al., 2014).  
352 This is due to the fact that the oxidation of GEM in the MBL must be photochemical, which have  
353 been evidenced by the diurnal cycle of RGM (Laurier and Mason, 2007). Another reason was that  
354 there was more Br (gas phase) production during daytime (Sander et al., 2003). Figure S3 showed  
355 that the RGM concentration in the nighttime was lower than those in corresponding forenoon and  
356 afternoon except the measurements in the PRE. This further indicated that: (1) the RGM

357 originated from the photo-oxidation of  $\text{Hg}^0$  in the atmosphere and (2) the transfer of RGM to  $\text{Hg}^{\text{P}}$   
358 due to higher RH and lower air temperature in nighttime (Rutter and Schauer, 2007; Lee et al.,  
359 2016).

360 In addition, we found that the difference in RGM concentration between day and night in the  
361 SCS was higher than those in the BS and YS (Wang et al., 2016b), and one possible reason was  
362 that the solar radiation and air temperature over the SCS were stronger and higher compared to  
363 those over the BS and YS (Wang et al., 2016b) as a result of the specific location of the SCS  
364 (tropical sea) and the different sampling season (the SCS: September 2015, the BS and YS:  
365 April–May and November 2014). Secondly, it could be found that the higher the RGM  
366 concentrations in the daytime, and the higher the RGM concentrations in the nighttime, but the  
367 concentrations in daytime were higher than that in the corresponding nighttime throughout the  
368 sampling period (see Figs. 7 and S3). This is partly because the higher RH and lower air  
369 temperature in nighttime were conducive to the removal of RGM (Rutter and Schauer, 2007;  
370 Amos et al., 2012). Thirdly, we found that the difference in RGM concentration between different  
371 days was large though there was no significantly difference in PAR values (Fig. 7). However, here  
372 again divide two kinds of cases: the first kind of circumstance was that the higher RGM in the  
373 PRE (day and night) presumably mainly originated from the surrounding human activities (i.e.,  
374 4–5 September 2015), and the second scenario was that RGM in open waters mainly originated  
375 from the in situ oxidation of GEM in the MBL (Soerensen et al., 2010a; Sprovieri et al., 2010).  
376 The main reason for the large difference in RGM concentration between different days was that  
377 there was large difference in wind speed and RH between different days (see Fig. 2), and the  
378 discussion can be found in the following paragraphs.

### 379 3.4.3 Daily variation of $\text{Hg}^{\text{P}}_{2.5}$

380 Figure 8 shows the  $\text{Hg}^{\text{P}}_{2.5}$  concentrations in the daytime and nighttime during the entire study  
381 period. The  $\text{Hg}^{\text{P}}_{2.5}$  value in the daytime ( $3.4 \pm 1.9 \text{ pg m}^{-3}$ ,  $n = 20$ ) was slightly but not significantly  
382 higher than that in the nighttime ( $2.4 \pm 0.9 \text{ pg m}^{-3}$ ,  $n = 19$ ) ( $t$ -test,  $p > 0.1$ ), and this pattern was  
383 consistent with the result of our previous study conducted in the open waters of YS (Wang et al.,  
384 2016b). The elevated  $\text{Hg}^{\text{P}}_{2.5}$  concentrations in the PRE and nearshore area of the Hainan Island  
385 (Figs. 4 and 8) indicated that the nearshore areas were readily polluted due to the anthropogenic  
386 Hg emissions, while the low  $\text{Hg}^{\text{P}}_{2.5}$  level in the open sea further suggested that the open areas of  
387 the SCS suffered less anthropogenic  $\text{Hg}^{\text{P}}$ . Therefore, we speculated that the  $\text{Hg}^{\text{P}}_{2.5}$  over the open  
388 SCS mainly originated from the in situ formation.

389 During the cruise in the western SCS (16–28 September 2015), we found elevated  $\text{Hg}^{\text{P}}_{2.5}$   
390 concentrations when the RGM concentrations were high at lower wind speed (e.g., 20–22  
391 September 2015, it was sunny all these days) (see Figs. 2, 7, 8). This is probably due to the  
392 transferring of RGM from the gas to the particle phase. In contrast, we found that the  $\text{Hg}^{\text{P}}_{2.5}$

393 concentrations were elevated when the RGM concentrations were low at higher wind speed (e.g.,  
394 25–27 September 2015, it was cloudy these days, and there was a transitory drizzly on 26  
395 September 2015) (see Figs. 2, 7 and 8). On the one hand, high wind speed may increase the levels  
396 of halogen atoms (Br and Cl etc.) and sea salt aerosols in the marine atmosphere, which in turn  
397 were favorable to the production of RGM and formation of  $\text{Hg}^{\text{P}}_{2.5}$  (Auzmendi-Murua et al., 2014).  
398 On the other hand, high wind speed was favorable to the removal of RGM and  $\text{Hg}^{\text{P}}_{2.5}$  in the  
399 atmosphere, this was probably the reason for lower RGM and  $\text{Hg}^{\text{P}}_{2.5}$  concentrations during 25–27  
400 September as compared to those observed during 20–22 September (see Figs. 2, 7 and 8).

### 401 **3.5 Relationship between atmospheric Hg and meteorological parameters**

402 Pearson's correlation coefficients were calculated between speciated Hg and meteorological  
403 parameters to identify the relationships between them (Table 2). According to the correlation  
404 analysis, the  $\text{Hg}^{\text{P}}_{2.5}$  was significantly positively correlated with RGM. Part of the reason was that  
405 RGM could be adsorbed by particulate matter under high RGM concentrations and then enhanced  
406 the  $\text{Hg}^{\text{P}}$  concentrations. Similarly, the  $\text{Hg}^{\text{P}}_{2.5}$  had a significantly positive correlation with GEM. On  
407 the one hand, GEM and  $\text{Hg}^{\text{P}}$  probably originated from the same sources (including but not limited  
408 to anthropogenic and oceanic sources) especially in the PRE and nearshore areas. On the other  
409 hand, it was probably due to the fact that GEM could be oxidized to form RGM and then  $\text{Hg}^{\text{P}}$ ,  
410 which might be the reason for the positive but not significant correlation between RGM and GEM  
411 since higher GEM level may result in higher RGM level in daytime.

412 The correlation analysis showed that the  $\text{Hg}^{\text{P}}_{2.5}$  and RGM were all negatively correlated with  
413 wind speed and RH (Table 2), and the higher wind speed was favorable to the removal of  $\text{Hg}^{\text{P}}_{2.5}$   
414 over the RGM. This is because the high wind speed might increase the RH levels and then  
415 elevated wind speed and RH may accelerate the removal of  $\text{Hg}^{\text{P}}_{2.5}$  and RGM (Cheng et al., 2014;  
416 Wang et al., 2016b). Moreover, both the air temperature and PAR were positively correlated with  
417 RGM and  $\text{Hg}^{\text{P}}_{2.5}$ . However, the significantly positive correlation between PAR and RGM  
418 indicated that the role of solar radiation played on the production of RGM was more obvious than  
419 that on the formation of  $\text{Hg}^{\text{P}}_{2.5}$ , which was consistent with the previous study at coastal and marine  
420 sites (Mao et al., 2012).

### 421 **3.6 Sea-air exchange of $\text{Hg}^0$ in the SCS**

422 The spatial distributions of DGM and  $\text{Hg}^0$  fluxes in the SCS were illustrated in Fig. 9. The DGM  
423 concentrations in nearshore area ( $40\text{--}55 \text{ pg l}^{-1}$ ) were about twice as high as those in the open sea,  
424 and this pattern was similar to our previous study conducted in the ECS (Wang et al., 2016c). The  
425 DGM concentration in this study varied from 23.0 to 66.8  $\text{pg l}^{-1}$  with a mean value of  $37.1 \pm 9.0$   
426  $\text{pg l}^{-1}$  (Fig. 9a and Table S3), which was higher than those in other open oceans, such as the  
427 Atlantic Ocean ( $11.6 \pm 2.0 \text{ pg l}^{-1}$ , Anderson et al., 2011), South Pacific Ocean ( $9\text{--}21 \text{ pg l}^{-1}$ ,

428 Soerensen et al., 2014), but considerably lower than that in the Minamata Bay ( $116 \pm 76 \text{ pg l}^{-1}$ ,  
429 Marumoto et al., 2015). The mean DGM concentration in the northern SCS ( $41.3 \pm 10.9 \text{ pg l}^{-1}$ )  
430 was significantly higher than that in the western SCS ( $33.5 \pm 5.0 \text{ pg l}^{-1}$ ) ( $t$ -test,  $p < 0.01$ ). The  
431 reason was that DGM concentrations in the nearshore areas of the PRE and Hainan Island were  
432 higher than those in the western open sea (see Fig. 9a). The DGM in surface seawater of the SCS  
433 was supersaturated with a saturation of 501 % to 1468 % with a mean value of  $903 \pm 208 \%$ ,  
434 which was approximately two thirds of that measured in the ECS (Wang et al., 2016c). The result  
435 indicated that: (1) the surface seawater in the SCS was supersaturated with gaseous Hg and (2)  
436 Hg<sup>0</sup> evaporated from the surface seawater to the atmosphere during our study period.

437 The sea-air exchange fluxes of Hg<sup>0</sup> at all stations were presented in Table S3, including GEM,  
438 DGM, PAR, surface seawater temperature, wind speed and saturation of Hg<sup>0</sup>. Sea-air exchange  
439 fluxes of Hg<sup>0</sup> in the SCS ranged from 0.40 to  $12.71 \text{ ng m}^{-2} \text{ h}^{-1}$  with a mean value of  $4.99 \pm 3.32$   
440  $\text{ng m}^{-2} \text{ h}^{-1}$  (Fig. 9b and Table S3), which was comparable to the previous measurements obtained  
441 in the Mediterranean Sea, northern SCS and West Atlantic Ocean (Andersson et al., 2007; Fu et al.,  
442 2010; Soerensen et al., 2013), but lower than those in polluted marine environments, such as the  
443 Minamata Bay, Tokyo Bay and YS (Narukawa et al., 2006; Ci et al., 2011; Marumoto et al., 2015),  
444 while higher than those in some open sea environments, such as the Baltic Sea, Atlantic Ocean and  
445 South Pacific Ocean (Kuss and Schneider, 2007; Andersson et al., 2011; Kuss et al., 2011;  
446 Soerensen et al., 2014). Interestingly, we found the Hg<sup>0</sup> flux near the station 99 were higher than  
447 those in open water as a result of higher wind speed (Table S3).

448 In order to better understand the important role of the SCS, we relate the Hg<sup>0</sup> flux in the SCS  
449 to the global estimation, an annual sea-air flux of Hg<sup>0</sup> was calculated based on the assumption that  
450 there was no seasonal variation in Hg<sup>0</sup> emission flux from the SCS. The annual emission flux of  
451 Hg<sup>0</sup> from the SCS was estimated to be  $159.6 \text{ tons yr}^{-1}$  assuming the area of the SCS was  $3.56 \times$   
452  $10^{12} \text{ m}^2$  (accounting for about 1.0 % of the global ocean area), which constituted about 5.5 % of  
453 the global Hg<sup>0</sup> oceanic evasion (Strode et al., 2007; Soerensen et al., 2010b; UNEP, 2013). We  
454 attributed the higher Hg<sup>0</sup> flux in the SCS to the specific location of the SCS (tropical sea) and the  
455 higher DGM concentrations in the SCS (especially in the northern area). Therefore, the SCS may  
456 actually play an important role in the global Hg oceanic cycle. Additionally, we found that the  
457 percentage of the annual dry deposition flux of atmospheric reactive Hg to the annual evasion flux  
458 of Hg<sup>0</sup> was approximately 18–34 %, indicating that the dry deposition of atmospheric reactive Hg  
459 was an important pathway for the atmospheric Hg to the ocean.

#### 460 **4 Conclusions**

461 During the cruise aboard the R/V *Shiyan 3* in September 2015, GEM, RGM and Hg<sup>P</sup> were  
462 determined in the MBL of the SCS. The GEM level in the SCS was comparable to the background  
463 level over the global oceans due to the air masses dominantly originated from seas and oceans.

464 GEM concentrations were closely related to the sources and movement patterns of air masses  
 465 during this cruise. Moreover, the speciated atmospheric Hg level in the PRE was significantly  
 466 higher than those in the open SCS due to the fresh emissions. The  $\text{Hg}^{\text{P}}$  concentrations in coarse  
 467 particles were significantly higher than those in fine particles, and the coarse modal was the  
 468 dominant size although there were three peaks for the size distribution of  $\text{Hg}^{\text{P}}$  in  $\text{PM}_{10}$ , indicating  
 469 that most of the  $\text{Hg}^{\text{P}}_{10}$  originated from in situ production. There was no significant difference in  
 470 GEM and  $\text{Hg}^{\text{P}}_{2.5}$  concentrations between day and night, but RGM concentrations were  
 471 significantly higher in daytime than in nighttime. RGM was positively correlated with PAR and air  
 472 temperature, but negatively correlated with wind speed and RH. The DGM concentrations in  
 473 nearshore areas of the SCS were higher than those in the open sea, and the surface seawater of the  
 474 SCS was supersaturated with respect to  $\text{Hg}^0$ . The annual flux of  $\text{Hg}^0$  from the SCS accounted for  
 475 about 5.5 % of the global  $\text{Hg}^0$  oceanic evasion although the area of the SCS just represents 1.0 %  
 476 of the global ocean area, suggesting that the SCS played an important role in the global Hg cycle.  
 477 Additionally, the dry deposition of atmospheric reactive Hg was a momentous pathway for the  
 478 atmospheric Hg to the ocean because it happens all the time.

## 479 5 Appendix A

480 **Table A1** List of acronyms and symbols

Abbreviation	Full name
BS	Bohai Sea
YS	Yellow Sea
ECS	East China Sea
SCS	South China Sea
PRE	Pearl River Estuary
MBL	Marine boundary layer
GEM	Gaseous elemental mercury
RGM	Reactive gaseous mercury
TAM	Total atmospheric mercury
$\text{Hg}^{\text{P}}_{2.1}$	Particulate mercury in $\text{PM}_{2.1}$
$\text{Hg}^{\text{P}}_{2.5}$	Particulate mercury in $\text{PM}_{2.5}$
$\text{Hg}^{\text{P}}_{10}$	Particulate mercury in $\text{PM}_{10}$
DGM	Dissolved gaseous mercury

481 Data are available from the first author Chunjie Wang (888wangchunjie888@163.com).

482 *Author contributions.* XZ and ZW designed the study. CW and FH organized the mercury  
 483 measurements. CW performed the data analysis, and wrote the paper. All authors contributed to  
 484 the manuscript with discussions and comments.

485 *Competing interests.* The authors declare that they have no conflict of interest.

486 *Acknowledgments.* This research was funded by the National Basic Research Program of China  
487 (No. 2013CB430002), National Natural Science Foundation of China (No. 41176066) and  
488 “Strategic Priority Research Program” of the Chinese Academy of Sciences, Grant No.  
489 XDB14020205. We gratefully acknowledge the open cruise organized by the South China Sea  
490 Institute of Oceanology, Chinese Academy of Sciences. The technical assistance of the staff of the  
491 R/V *Shiyan 3* is gratefully acknowledged.

## 492 **References**

- 493 Ahn, M. C., Kim, B., Holsen, T. M., Yi, S. M., and Han, Y. J.: Factors influencing concentrations of dissolved  
494 gaseous mercury (DGM) and total mercury (TM) in an artificial reservoir, *Environ. Pollut.*, 158, 347–355,  
495 <https://doi.org/10.1016/j.envpol.2009.08.036>, 2010.
- 496 Amos, H. M., Jacob, D. J., Holmes, C. D., Fisher, J. A., Wang, Q., Yantosca, R. M., Corbitt, E. S., Galarneau, E.,  
497 Rutter, A. P., Gustin, M. S., Steffen, A., Schauer, J. J., Graydon, J. A., St. Louis, V. L., Talbot, R. W., Edgerton, E.  
498 S., Zhang, Y., and Sunderland, E. M.: Gas-particle partitioning of atmospheric Hg(II) and its effect on global  
499 mercury deposition, *Atmos. Chem. Phys.*, 12, 591–603, <https://doi.org/10.5194/acp-12-591-2012>, 2012.
- 500 Andersson, M. E., Gårdfeldt, K., Wängberg, I., Sprovieri, F., Pirrone, N., and Lindqvist, O.: Seasonal and daily  
501 variation of mercury evasion at coastal and off shore sites from the Mediterranean Sea, *Mar. Chem.*, 104,  
502 214–226, <https://doi.org/10.1016/j.marchem.2006.11.003>, 2007.
- 503 Andersson, M. E., Sommar, J., Gårdfeldt, K., and Jutterström, S.: Air–sea exchange of volatile mercury in the  
504 North Atlantic Ocean, *Mar. Chem.*, 125, 1–7, <https://doi.org/10.1016/j.marchem.2011.01.005>, 2011.
- 505 Angot, H., Barret, M., Magand, O., Ramonet, M., Dommergue, A.: A 2-year record of atmospheric mercury  
506 species at a background Southern Hemisphere station on Amsterdam Island, *Atmos. Chem. Phys.*, 14,  
507 11461–11473, <https://doi.org/10.5194/acp-14-11461-2014>, 2014
- 508 Ariya, P. A., Amyot, M., Dastoor, A., Deeds, D., Feinberg, A., Kos, G., Poulain, A., Ryjkov, A., Semeniuk, K.,  
509 Subir, M., and Toyota, K.: Mercury physicochemical and biogeochemical transformation in the atmosphere and  
510 at atmospheric interfaces: A review and future directions, *Chem. Rev.*, 115, 3760–3802,  
511 <https://doi.org/10.1021/cr500667e>, 2015.
- 512 Athanasopoulou, E., Tombrou, M., Pandis, S. N., and Russell, A. G.: The role of sea-salt emissions and  
513 heterogeneous chemistry in the air quality of polluted coastal areas, *Atmos. Chem. Phys.*, 8, 5755–5769,  
514 <https://doi.org/10.5194/acp-8-5755-2008>, 2008.
- 515 Auzmendi-Murua, I., Castillo, Á., and Bozzelli, J. W.: Mercury oxidation via chlorine, bromine, and iodine under  
516 atmospheric conditions: Thermochemistry and kinetics, *J. Phys. Chem. A*, 118, 2959–2975,  
517 <https://doi.org/10.1021/jp412654s>, 2014.
- 518 Bowman, K. L., Hammerschmidt, C. R., Lamborg, C. H., and Swarr, G.: Mercury in the North Atlantic Ocean: The  
519 U.S. GEOTRACES zonal and meridional sections, *Deep Sea Res. Part II*, 116, 251–261,  
520 <https://doi.org/10.1016/j.dsr2.2014.07.004>, 2015.

521 Chand, D., Jaffe, D., Prestbo, E., Swartzendruber, P. C., Hafner, W., Weiss-Penzias, P., Kato, S., Takami, A.,  
522 Hatakeyama, S., and Kajii, Y.: Reactive and particulate mercury in the Asian marine boundary layer, *Atmos.*  
523 *Environ.*, 42, 7988–7996, <https://doi.org/10.1016/j.atmosenv.2008.06.048>, 2008.

524 Cheng, I., Zhang, L., Blanchard, P., Graydon, J. A., and St. Louis, V. L.: Source-receptor relationships for speciated  
525 atmospheric mercury at the remote Experimental Lakes Area, northwestern Ontario, Canada, *Atmos. Chem.*  
526 *Phys.*, 12, 1903–1922, <https://doi.org/10.5194/acp-12-1903-2012>, 2012.

527 Cheng, I., Zhang, L., Blanchard, P., Dalziel, J., Tordon, R., Huang, J., and Holsen, T. M.: Comparisons of mercury  
528 sources and atmospheric mercury processes between a coastal and inland site, *J. Geophys. Res.*, 118, 2434–2443,  
529 <https://doi.org/10.1002/jgrd.50169>, 2013.

530 Cheng, I., Zhang, L., Mao, H., Blanchard, P., Tordon, R., and Dalziel, J.: Seasonal and diurnal patterns of speciated  
531 atmospheric mercury at a coastal-rural and a coastal-urban site, *Atmos. Environ.*, 82, 193–205,  
532 <https://doi.org/10.1016/j.atmosenv.2013.10.016>, 2014.

533 Ci, Z., Zhang, X., Wang, Z., Niu, Z., Diao, X., and Wang, S.: Distribution and air–sea exchange of mercury (Hg) in  
534 the Yellow Sea, *Atmos. Chem. Phys.*, 11, 2881–2892, <https://doi.org/10.5194/acp-11-2881-2011>, 2011.

535 Ci, Z., Wang, C., Wang, Z., and Zhang, X.: Elemental mercury (Hg(0)) in air and surface waters of the Yellow Sea  
536 during late spring and late fall 2012: Concentration, spatial-temporal distribution and air/sea flux, *Chemosphere*,  
537 119, 199–208, <https://doi.org/10.1016/j.chemosphere.2014.05.064>, 2015.

538 de Foy, B., Tong, Y., Yin, X., Zhang, W., Kang, S., Zhang, Q., Zhang, G., Wang, X., and Schauer, J. J.: First  
539 field-based atmospheric observation of the reduction of reactive mercury driven by sunlight, *Atmos. Environ.*,  
540 134, 27–39, <https://doi.org/10.1016/j.atmosenv.2016.03.028>, 2016.

541 Draxler, R. R., and Rolph, G. D.: HYSPLITModel access via NOAA ARL READY Website  
542 (<http://www.arl.noaa.gov/ready/hysplit4.html>), NOAA Air Resources Laboratory, Silver Spring, MD, 2012.

543 Engle, M. A., Tate, M. T., Krabbenhoft, D. P., Kolker, A., Olson, M. L., Edgerton, E. S., DeWild, J. F., and  
544 McPherson, A. K.: Characterization and cycling of atmospheric mercury along the central US Gulf Coast, *Appl.*  
545 *Geochem.*, 23, 419–437, <https://doi.org/10.1016/j.apgeochem.2007.12.024>, 2008.

546 Feddersen, D. M., Talbot, R., Mao, H., and Sive, B. C.: Size distribution of particulate mercury in marine and  
547 coastal atmospheres, *Atmos. Chem. Phys.*, 12, 10899–10909, <https://doi.org/10.5194/acp-12-10899-2012>, 2012.

548 Fu, X., Feng, X., Zhang, G., Xu, W., Li, X., Yao, H., Liang, P., Li, J., Sommar, J., Yin, R., and Liu, N.: Mercury in  
549 the marine boundary layer and seawater of the South China Sea: Concentrations, sea/air flux, and implication for  
550 land outflow, *J. Geophys. Res.*, 115, D06303, <https://doi.org/10.1029/2009JD012958>, 2010.

551 Fu, X., Feng, X., Qiu, G., Shang, L., and Zhang, H.: Speciated atmospheric mercury and its potential source in  
552 Guiyang, China, *Atmos. Environ.*, 45, 4205–4212, <https://doi.org/10.1016/j.atmosenv.2011.05.012>, 2011.

553 Fu, X., Feng, X., Liang, P., Deliger, Zhang, H., Ji, J., and Liu, P.: Temporal trend and sources of speciated  
554 atmospheric mercury at Waliguan GAW station, Northwestern China, *Atmos. Chem. Phys.*, 12, 1951–1964,  
555 <https://doi.org/10.5194/acp-12-1951-2012>, 2012.

556 Giorgi, F.: Dry deposition velocities of atmospheric aerosols as inferred by applying a particle dry deposition  
557 parameterisation to a general circulation model, *Tellus*, 40B, 23–41,



558 <https://doi.org/10.1111/j.1600-0889.1988.tb00210.x>, 1988.

559 Gratz, L. E., Ambrose, J. L., Jaffe, D. A., Shah, V., Jaegle, L., Stutz, J., Festa, J., Spolaor, M., Tsai, C., Selin, N. E.,  
560 Song, S., Zhou, X., Weinheimer, A. J., Knapp, D. J., Montzka, D. D., Flocke, F. M., Campos, T. L., Apel, E.,  
561 Hornbrook, R., Blake, N. J., Hall, S., Tyndall, G. S., Reeves, M., Stechman, D., and Stell, M.: Oxidation of  
562 mercury by bromine in the subtropical Pacific free troposphere, *Geophys. Res. Lett.*, 42, 10494–10502,  
563 <https://doi.org/10.1002/2015GL066645>, 2015.

564 Gustin, M. S., Huang, J., Miller, M. B., Peterson, C., Jaffe, D. A., Ambrose, J., Finley, B. D., Lyman, S. N., Call,  
565 K., Talbot, R., Feddersen, D., Mao, H., and Lindberg, S. E.: Do we understand what the mercury speciation  
566 instruments are actually measuring? Results of RAMIX, *Environ. Sci. Technol.*, 47, 7295–7306,  
567 <https://doi.org/10.1021/es3039104>, 2013.

568 Hedgecock, I. and Pirrone, N.: Mercury and photochemistry in the marine boundary layer-modelling studies  
569 suggest the in situ production of reactive gas phase mercury, *Atmos. Environ.*, 35, 3055–3062,  
570 [https://doi.org/10.1016/S1352-2310\(01\)00109-1](https://doi.org/10.1016/S1352-2310(01)00109-1), 2001.

571 Holmes, C. D., Jacob, D. J., and Yang, X.: Global lifetime of elemental mercury against oxidation by atomic  
572 bromine in the free troposphere, *Geophys. Res. Lett.*, 33, L20808, <https://doi.org/10.1029/2006gl027176>, 2006.

573 Holmes, C. D., Jacob, D. J., Mason, R. P., and Jaffe, D. A.: Sources and deposition of reactive gaseous mercury in  
574 the marine atmosphere, *Atmos. Environ.*, 43, 2278–2285, <https://doi.org/10.1016/j.atmosenv.2009.01.051>, 2009.

575 Holmes, C. D., Jacob, D. J., Corbitt, E. S., Mao, J., Yang, X., Talbot, R., and Slemr, F.: Global atmospheric model  
576 for mercury including oxidation by bromine atoms, *Atmos. Chem. Phys.*, 10, 12037–12057,  
577 <https://doi.org/10.5194/acp-10-12037-2010>, 2010.

578 Horowitz, H. M., Jacob, D. J., Zhang, Y., Dibble, T. S., Slemr, F., Amos, H. M., Schmidt, J. A., Corbitt, E. S.,  
579 Marais, E. A., and Sunderland, E. M.: A new mechanism for atmospheric mercury redox chemistry: implications  
580 for the global mercury budget, *Atmos. Chem. Phys.*, 17, 6353–6371, <https://doi.org/10.5194/acp-17-6353-2017>,  
581 2017.

582 Horvat, M., Kotnik, J., Logar, M., Fajon, V., Zvonarić, T., and Pirrone, N.: Speciation of mercury in surface and  
583 deep-sea waters in the Mediterranean Sea, *Atmos. Environ.*, 37, S93–S108,  
584 [https://doi.org/10.1016/S1352-2310\(03\)00249-8](https://doi.org/10.1016/S1352-2310(03)00249-8), 2003.

585 Howard, D., Nelson, P. F., Edwards, G. C., Morrison, A. L., Fisher, J. A., Ward, J., Harnwell, J., van der Schoot, M.,  
586 Atkinson, B., Chambers, S. D., Griffiths, A. D., Werczynski, S., and Williams, A. G.: Atmospheric mercury in  
587 the Southern Hemisphere tropics: seasonal and diurnal variations and influence of inter-hemispheric transport,  
588 *Atmos. Chem. Phys.*, 17, 11623–11636, <https://doi.org/10.5194/acp-17-11623-2017>, 2017.

589 Huang, J., Miller, M. B., Edgerton, E., and Sexauer Gustin, M.: Deciphering potential chemical compounds of  
590 gaseous oxidized mercury in Florida, USA, *Atmos. Chem. Phys.*, 17, 1689–1698,  
591 <https://doi.org/10.5194/acp-17-1689-2017>, 2017.

592 Kim, S. H., Han, Y. J., Holsen, T. M., and Yi, S. M.: Characteristics of atmospheric speciated mercury  
593 concentrations (TGM, Hg(II) and Hg(p)) in Seoul, Korea, *Atmos. Environ.*, 43, 3267–3274,  
594 <https://doi.org/10.1016/j.atmosenv.2009.02.038>, 2009.

595 Kim, P. R., Han, Y. J., Holsen, T. M., and Yi, S. M.: Atmospheric particulate mercury: Concentrations and size  
596 distributions, *Atmos. Environ.*, 61, 94–102, <https://doi.org/10.1016/j.atmosenv.2012.07.014>, 2012.

597 Kuss, J.: Water–air gas exchange of elemental mercury: An experimentally determined mercury diffusion  
598 coefficient for  $\text{Hg}^0$  water–air flux calculations, *Limnol. Oceanogr.*, 59, 1461–1467,  
599 <https://doi.org/10.4319/lo.2014.59.5.1461>, 2014.

600 Kuss, J., and Schneider, B.: Variability of the gaseous elemental mercury sea-air flux of the Baltic Sea, *Environ.*  
601 *Sci. Technol.*, 41, 8018–8023, <https://doi.org/10.1021/es0716251>, 2007.

602 Kuss, J., Züllicke, C., Pohl, C., and Schneider, B.: Atlantic mercury emission determined from continuous analysis  
603 of the elemental mercury sea-air concentration difference within transects between 50°N and 50°S, *Global*  
604 *Biogeochem. Cycles*, 25, GB 3021, <https://doi.org/10.1029/2010GB003998>, 2011.

605 Kuss, J., Krüger, S., Ruickoldt, J., and Wlost, K.-P.: High-resolution measurements of elemental mercury in  
606 surface water for an improved quantitative understanding of the Baltic Sea as a source of atmospheric mercury,  
607 *Atmos. Chem. Phys.*, 18, 4361–4376, <https://doi.org/10.5194/acp-18-4361-2018>, 2018.

608 Landis, M. S., Stevens, R. K., Schaedlich, F., and Prestbo, E. M.: Development and characterization of an annular  
609 denuder methodology for the measurement of divalent inorganic reactive gaseous mercury in ambient air,  
610 *Environ. Sci. Technol.*, 36, 3000–3009, <https://doi.org/10.1021/es015887t>, 2002.

611 Laurier, F. J. G., Mason, R. P., Whalin, L., and Kato, S.: Reactive gaseous mercury formation in the North Pacific  
612 Ocean’s marine boundary layer: A potential role of halogen chemistry, *J. Geophys. Res.*, 108, 4529,  
613 <https://doi.org/10.1029/2003JD003625>, 2003.

614 Laurier, F., and Mason, R.: Mercury concentration and speciation in the coastal and open ocean boundary layer, *J.*  
615 *Geophys. Res.*, 112, D06302, <https://doi.org/10.1029/2006JD007320>, 2007.

616 Lee, G.-S., Kim, P.-R., Han, Y.-J., Holsen, T. M., Seo, Y.-S., and Yi, S.-M.: Atmospheric speciated mercury  
617 concentrations on an island between China and Korea: sources and transport pathways, *Atmos. Chem. Phys.*, 16,  
618 4119–4133, <https://doi.org/10.5194/acp-16-4119-2016>, 2016.

619 Lindberg, S. E., Brooks, S., Lin, C. J., Scott, K. J., Landis, M. S., Stevens, R. K., Goodsite, M., and Richter, A.:  
620 Dynamic oxidation of gaseous mercury in the Arctic troposphere at polar sunrise, *Environ. Sci. Technol.*, 36,  
621 1245–1256, <https://doi.org/10.1021/es0111941>, 2002.

622 Liss, P. W., and Slater, P. G.: Flux of gases across the air-sea interface, *Nature*, 247, 181–184,  
623 <https://doi.org/10.1038/247181a0>, 1974.

624 Liu, B., Keeler, G. J., Dvonch, J. T., Barres, J. A., Lynam, M. M., Marsik, F. J., and Morgan, J. T.: Temporal  
625 variability of mercury speciation in urban air, *Atmos. Environ.*, 41, 1911–1923,  
626 <https://doi.org/10.1016/j.atmosenv.2006.10.063>, 2007.

627 Liu, B., Keeler, G. J., Dvonch, J. T., Barres, J. A., Lynam, M. M., Marsik, F. J., and Morgan, J. T.: Urban-rural  
628 differences in atmospheric mercury speciation, *Atmos. Environ.*, 44, 2013–2023,  
629 <https://doi.org/10.1016/j.atmosenv.2010.02.012>, 2010.

630 Liu, N., Qiu, G., Landis, M., Feng, X., Fu, X., and Shang, L.: Atmospheric mercury species measured in Guiyang,  
631 Guizhou province, southwest China, *Atmos. Res.*, 100, 93–102, <https://doi.org/10.1016/j.atmosres.2011.01.002>,

632 2011.

633 Mamane, Y., Perrino, C., Yossef, O., and Catrambone, M.: Source characterization of fine and coarse particles at  
634 the East mediterranean coast, *Atmos. Environ.*, 42, 6114–6130, doi:10.1016/j.atmosenv.2008.02.045, 2008.

635 Mao, H., Talbot, R., Hegarty, J., and Koerner, J.: Speciated mercury at marine, coastal, and inland sites in New  
636 England – Part 2: Relationships with atmospheric physical parameters, *Atmos. Chem. Phys.*, 12, 4181–4206,  
637 <https://doi.org/10.5194/acp-12-4181-2012>, 2012.

638 Mao, H., Cheng, I., and Zhang, L.: Current understanding of the driving mechanisms for spatiotemporal variations  
639 of atmospheric speciated mercury: a review, *Atmos. Chem. Phys.*, 16, 12897–12924,  
640 <https://doi.org/10.5194/acp-16-12897-2016>, 2016.

641 Mao, H., Hall, D., Ye, Z., Zhou, Y., Felton, D., and Zhang, L.: Impacts of large-scale circulation on urban ambient  
642 concentrations of gaseous elemental mercury in New York, USA, *Atmos. Chem. Phys.*, 17, 11655–11671,  
643 <https://doi.org/10.5194/acp-17-11655-2017>, 2017.

644 Marumoto, K., and Imai, S.: Determination of dissolved gaseous mercury in seawater of Minamata Bay and  
645 estimation for mercury exchange across air–sea interface, *Mar. Chem.*, 168, 9–17,  
646 <https://doi.org/10.1016/j.marchem.2014.09.007>, 2015.

647 Mason, R. P., Choi, A. L., Fitzgerald, W. F., Hammerschmidt, C. R., Lamborg, C. H., Soerensen, A. L., and  
648 Sunderland, E. M.: Mercury biogeochemical cycling in the ocean and policy implications, *Environ. Res.*, 119,  
649 101–117, doi:10.1016/j.envres.2012.03.013, 2012.

650 Mason, R. P., Hammerschmidt, C. R., Lamborg, C. H., Bowman, K. L., Swarr, G. J., and Shelley, R. U.: The air-sea  
651 exchange of mercury in the low latitude Pacific and Atlantic Oceans, *Deep Sea Res. Part I*, 122, 17–28,  
652 <https://doi.org/10.1016/j.dsr.2017.01.015>, 2017.

653 Narukawa, M., Sakata, M., Marumoto, K., and Asakura, K.: Air-sea exchange of mercury in Tokyo Bay, *J.*  
654 *Oceanogr.*, 62, 249–257, <https://doi.org/10.1007/s10872-006-0049-3>, 2006.

655 Nho-Kim, E. Y., Michou, M., and Peuch, V. H.: Parameterization of size-dependent particle dry deposition  
656 velocities for global modeling, *Atmos. Environ.*, 38, 1933–1942, <https://doi.org/10.1016/j.atmosenv.2004.01.002>,  
657 2004.

658 Poissant, L., Pilote, M., Xu, X., Zhang, H. and Beauvais C.: Atmospheric mercury speciation and deposition in the  
659 Bay St. François wetlands, *J. Geophys. Res.*, 109, D11301, <https://doi.org/10.1029/2003JD004364>, 2004.

660 Pryor, S. C., and Sorensen, L. L.: Nitric acid-sea salt reactions: Implications for nitrogen deposition to water  
661 surfaces, *J. Appl. Meteorol.*, 39, 725–731, <https://doi.org/10.1175/1520-0450-39.5.725>, 2000.

662 Radke, L. F., Friedli, H. R., and Heikes, B. G.: Atmospheric mercury over the NE Pacific during spring 2002:  
663 Gradients, residence time, upper troposphere lower stratosphere loss, and long-range transport, *J. Geophys. Res.*,  
664 112, D19305, <https://doi.org/10.1029/2005JD005828>, 2007.

665 Read, K. A., Neves, L. M., Carpenter, L. J., Lewis, A. C., Fleming, Z. L., and Kentisbeer, J.: Four years  
666 (2011–2015) of total gaseous mercury measurements from the Cape Verde Atmospheric Observatory, *Atmos.*  
667 *Chem. Phys.*, 17, 5393–5406, <https://doi.org/10.5194/acp-17-5393-2017>, 2017.

668 Rutter, A. P., and Schauer, J. J.: The effect of temperature on the gas–particle partitioning of reactive mercury in

669 atmospheric aerosols, *Atmos. Environ.*, 41, 8647–8657, <https://doi.org/10.1016/j.atmosenv.2007.07.024>, 2007.

670 Sander, R., Keene, W. C., Pszenny, A. A. P., Arimoto, R., Ayers, G. P., Baboukas, E., Cainey, J. M., Crutzen, P. J.,  
671 Duce, R. A., Hönninger, G., Huebert, B. J., Maenhaut, W., Mihalopoulos, N., Turekian, V. C., and Van Dingenen,  
672 R., Inorganic bromine in the marine boundary layer: a critical review, *Atmos. Chem. Phys.*, 3, 1301–1336,  
673 <https://doi.org/10.5194/acp-3-1301-2003>, 2003.

674 Schroeder, W. H., and Munthe, J.: Atmospheric mercury – An overview, *Atmos. Environ.*, 32, 809–822,  
675 [https://doi.org/10.1016/S1352-2310\(97\)00293-8](https://doi.org/10.1016/S1352-2310(97)00293-8), 1998.

676 Selin, N. E., Jacob, D. J., Park, R. J., Yantosca, R. M., Strode, S., Jaeglé L., and Jaffe, D.: Chemical cycling and  
677 deposition of atmospheric mercury: Global constraints from observations, *J. Geophys. Res.*, 112, D02308,  
678 <https://doi.org/10.1029/2006JD007450>, 2007.

679 Shah, V., Jaeglé L., Gratz, L. E., Ambrose, J. L., Jaffe, D. A., Selin, N. E., Song, S., Campos, T. L., Flocke, F. M.,  
680 Reeves, M., Stechman, D., Stell, M., Festa, J., Stutz, J., Weinheimer, A. J., Knapp, D. J., Montzka, D. D.,  
681 Tyndall, G. S., Apel, E. C., Hornbrook, R. S., Hills, A. J., Riemer, D. D., Blake, N. J., Cantrell, C. A., and  
682 Mauldin III, R. L.: Origin of oxidized mercury in the summertime free troposphere over the southeastern US,  
683 *Atmos. Chem. Phys.*, 16, 1511–1530, <https://doi.org/10.5194/acp-16-1511-2016>, 2016.

684 Sheu, G. R., and Mason, R. P.: An examination of the oxidation of elemental mercury in the presence of halide  
685 surfaces, *J. Atmos. Chem.*, 48, 107–130, <https://doi.org/10.1023/B:JOCH.0000036842.37053.e6>, 2004.

686 Slemr, F., Angot, H., Dommergue, A., Magand, O., Barret, M., Weigelt, A., Ebinghaus, R., Brunke, E.-G.,  
687 Pfaffhuber, K. A., Edwards, G., Howard, D., Powell, J., Keywood, M., and Wang, F.: Comparison of mercury  
688 concentrations measured at several sites in the Southern Hemisphere, *Atmos. Chem. Phys.*, 15, 3125–3133,  
689 <https://doi.org/10.5194/acp-15-3125-2015>, 2015.

690 Soerensen, A. L., Skov, H., Jacob, D. J., Soerensen, B. T., and Johnson, M. S.: Global concentrations of gaseous  
691 elemental mercury and reactive gaseous mercury in the marine boundary layer, *Environ. Sci. Technol.*, 44,  
692 7425–7430, <https://doi.org/10.1021/es903839n>, 2010a.

693 Soerensen, A. L., Sunderland, E. M., Holmes, C. D., Jacob, D. J., Yantosca, R. M., Skov, H., Christensen, J. H.,  
694 Strode, S. A., and Mason, R. P.: An improved global model for air-sea exchange of mercury: high concentrations  
695 over the North Atlantic, *Environ. Sci. Technol.*, 44, 8574–8580, <https://doi.org/10.1021/es102032g>, 2010b.

696 Soerensen, A. L., Mason, R. P., Balcom, P. H., and Sunderland, E. M.: Drivers of surface ocean mercury  
697 concentrations and air–sea exchange in the west Atlantic Ocean, *Environ. Sci. Technol.*, 47, 7757–7765,  
698 <https://doi.org/10.1021/es401354q>, 2013.

699 Soerensen, A. L., Mason, R. P., Balcom, P. H., Jacob, D. J., Zhang, Y., Kuss, J., and Sunderland, E. M.: Elemental  
700 mercury concentrations and fluxes in the tropical atmosphere and ocean, *Environ. Sci. Technol.*, 48,  
701 11312–11319, <https://doi.org/10.1021/es503109p>, 2014.

702 Sprovieri, F., Pirrone, N., Gärdfeldt, K., and Sommar, J.: Mercury speciation in the marine boundary layer along a  
703 6000 km cruise path around the Mediterranean Sea, *Atmos. Environ.*, 37, S63–S71,  
704 [https://doi.org/10.1016/S1352-2310\(03\)00237-1](https://doi.org/10.1016/S1352-2310(03)00237-1), 2003.

705 Sprovieri, F., and Pirrone, N.: Spatial and temporal distribution of atmospheric mercury species over the Adriatic

706 Sea, *Environ. Fluid Mech.*, 8, 117–128, <https://doi.org/10.1007/s10652-007-9045-4>, 2008.

707 Sprovieri, F., Hedgecock, I. M., and Pirrone, N.: An investigation of the origins of reactive gaseous mercury in the  
708 Mediterranean marine boundary layer, *Atmos. Chem. Phys.*, 10, 3985–3997,  
709 <https://doi.org/10.5194/acp-10-3985-2010>, 2010.

710 Steffen, A., Lehnher, I., Cole, A., Ariya, P., Dastoor, A., Durnford, D., Kirk, J., and Pilote, M.: Atmospheric  
711 mercury measurements in the Canadian Arctic Part 1: A review of recent field measurements, *Sci. Total Environ.*,  
712 509–510, 3–15, <https://doi.org/10.1016/j.scitotenv.2014.10.109>, 2015.

713 Strode, S. A., Jaeglé L., Selin, N. E., Jacob, D. J., Park, R. J., Yantosca, R. M., Mason, R. P., and Slemr, F.: Air-sea  
714 exchange in the global mercury cycle, *Global Biogeochem. Cycles*, 21, GB1017,  
715 <https://doi.org/10.1029/2006GB002766>, 2007.

716 Tseng, C. M., Liu, C. S., and Lamborg, C.: Seasonal changes in gaseous elemental mercury in relation to monsoon  
717 cycling over the northern South China Sea, *Atmos. Chem. Phys.*, 12, 7341–7350,  
718 <https://doi.org/10.5194/acp-12-7341-2012>, 2012.

719 UNEP: Global Mercury Assessment: Sources, Emissions, Releases and Environmental Transport, UNEP  
720 Chemicals Branch, Geneva, Switzerland, 2013.

721 Valente, R. J., Shea, C., Humes, K. L., and Tanner, R. L.: Atmospheric mercury in the Great Smoky Mountains  
722 compared to regional and global levels, *Atmos. Environ.*, 41, 1861–1873,  
723 <https://doi.org/10.1016/j.atmosenv.2006.10.054>, 2007.

724 Wang, Y. Q., Zhang, X. Y., and Draxler, R. R.: TrajStat: GIS-based software that uses various trajectory statistical  
725 analysis methods to identify potential sources from long-term air pollution measurement data, *Environ. Model.*  
726 *Softw.*, 28, 938–939, <https://doi.org/10.1016/j.envsoft.2009.01.004>, 2009.

727 Wang, S., Schmidt, J. A., Baidar, S., Coburn, S., Dix, B., Koenig, T. K., Apel, E., Bowdalo, D., Campos, T. L.,  
728 Eloranta, E., Evans, M. J., DiGangi, J. P., Zondlo, M. A., Gao, R. S., Haggerty, J. A., Hall, S. R., Hornbrook, R.  
729 S., Jacob, D., Morley, B., Pierce, B., Reeves, M., Romashkin, P., ter Schure, A., and Volkamer, R.: Active and  
730 widespread halogen chemistry in the tropical and subtropical free troposphere, *Proc. Natl. Acad. Sci. U.S.A.*,  
731 112, 9281–9286, <https://doi.org/10.1073/pnas.1505142112>, 2015.

732 Wang, C., Wang, Z., Ci, Z., Zhang, X., and Tang, X.: Spatial-temporal distributions of gaseous element mercury  
733 and particulate mercury in the Asian marine boundary layer, *Atmos. Environ.*, 126, 107–116,  
734 <https://doi.org/10.1016/j.atmosenv.2015.11.036>, 2016a.

735 Wang, C., Ci, Z., Wang, Z., Zhang, X., and Guo, J.: Speciated atmospheric mercury in the marine boundary layer  
736 of the Bohai Sea and Yellow Sea, *Atmos. Environ.*, 131, 360–370,  
737 <https://doi.org/10.1016/j.atmosenv.2016.02.021>, 2016b.

738 Wang, C., Ci, Z., Wang, Z., and Zhang, X.: Air-sea exchange of gaseous mercury in the East China Sea, *Environ.*  
739 *Pollut.*, 212, 535–543, <https://doi.org/10.1016/j.envpol.2016.03.016>, 2016c.

740 Wanninkhof, R.: Relationship between wind speed and gas exchange over the ocean, *J. Geophys. Res.*, 97,  
741 7373–7382, <https://doi.org/10.1029/92JC00188>, 1992.

742 Witt, M. L. I., Mather, T. A., Baker, A. R., De Hoog, J. C. M., and Pyle, D. M.: Atmospheric trace metals over the

743 south-west Indian Ocean: Total gaseous mercury, aerosol trace metal concentrations and lead isotope ratios, *Mar.*  
 744 *Chem.*, 121, 2–16, <https://doi.org/10.1016/j.marchem.2010.02.005>, 2010.

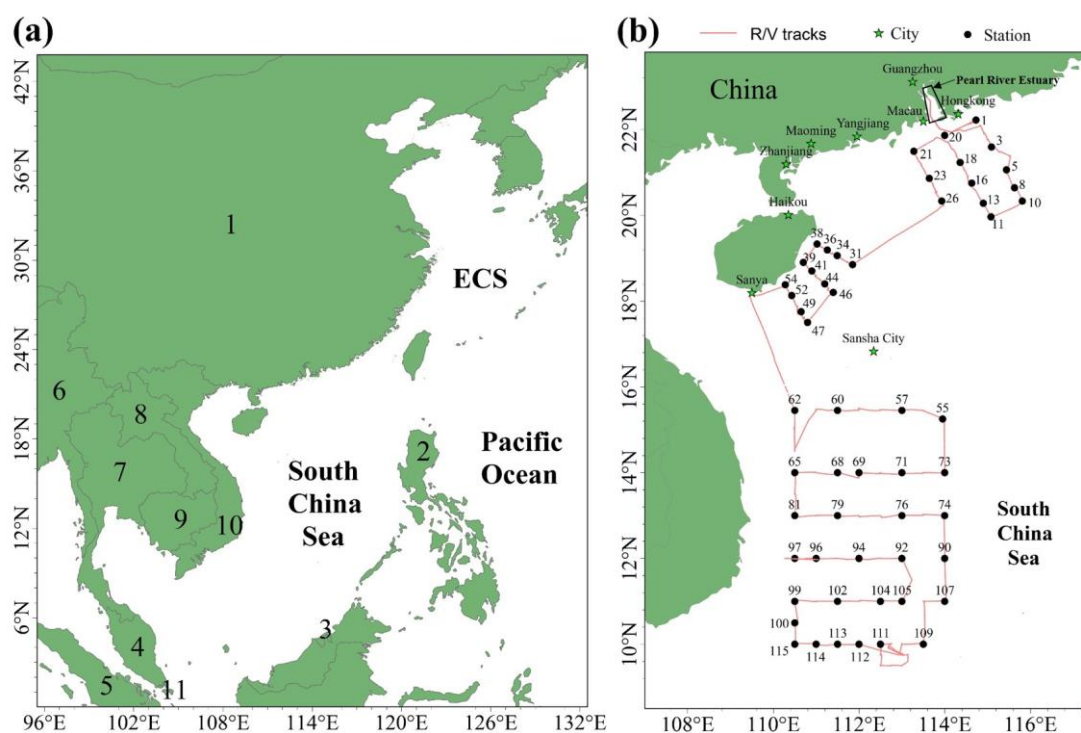
745 Xu, L., Chen, J., Yang, L., Niu, Z., Tong, L., Yin, L., and Chen, Y.: Characteristics and sources of atmospheric  
 746 mercury speciation in a coastal city, Xiamen, China, *Chemosphere*, 119, 530–539,  
 747 <https://doi.org/10.1016/j.chemosphere.2014.07.024>, 2015.

748 Ye, Z., Mao, H., Lin, C.-J., and Kim, S. Y.: Investigation of processes controlling summertime gaseous elemental  
 749 mercury oxidation at midlatitudinal marine, coastal, and inland sites, *Atmos. Chem. Phys.*, 16, 8461–8478,  
 750 <https://doi.org/10.5194/acp-16-8461-2016>, 2016.

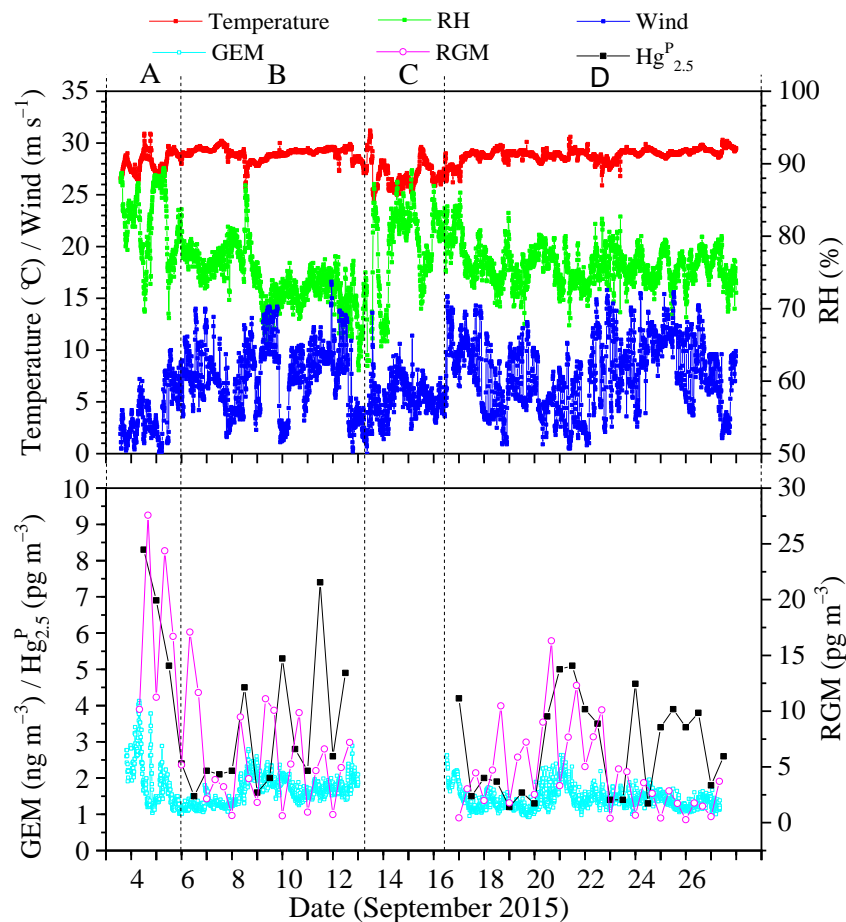
751 Zhu, J., Wang, T., Talbot, R., Mao, H., Yang, X., Fu, C., Sun, J., Zhuang, B., Li, S., Han, Y., and Xie, M.:  
 752 Characteristics of atmospheric mercury deposition and size-fractionated particulate mercury in urban Nanjing,  
 753 China, *Atmos. Chem. Phys.*, 14, 2233–2244, <https://doi.org/10.5194/acp-14-2233-2014>, 2014.

754

755 **Figures and Tables**

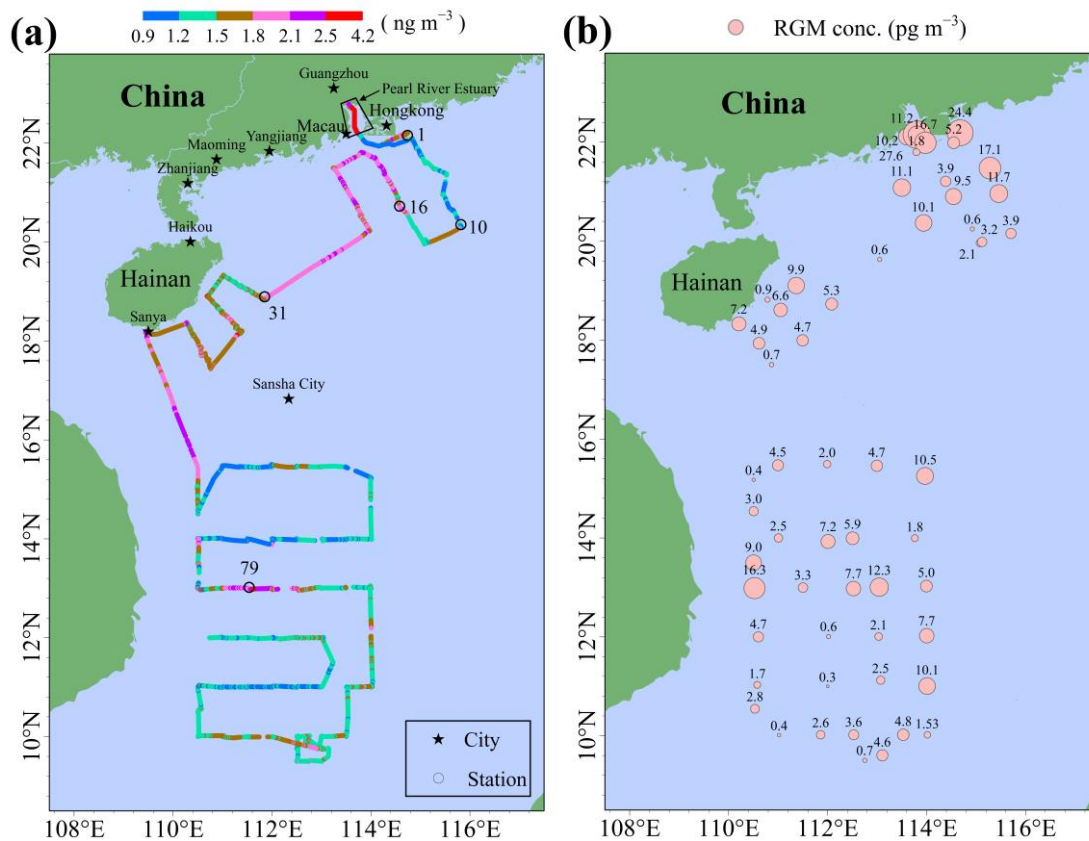


756 **Figure 1.** Map of the South China Sea (a) (1: China, 2: Philippines, 3: Brunei, 4: Malaysia, 5:  
 757 Indonesia, 6: Myanmar, 7: Thailand, 8: Laos, 9: Cambodia, 10: Vietnam, 11: Singapore). The  
 758 locations of the Pearl River Estuary (PRE), DGM sampling stations and R/V tracks (b). It should  
 759 be noted that the black solid points represent the sampling stations, and the number near the black  
 760 solid point represents the name of the station.  
 761  
 762



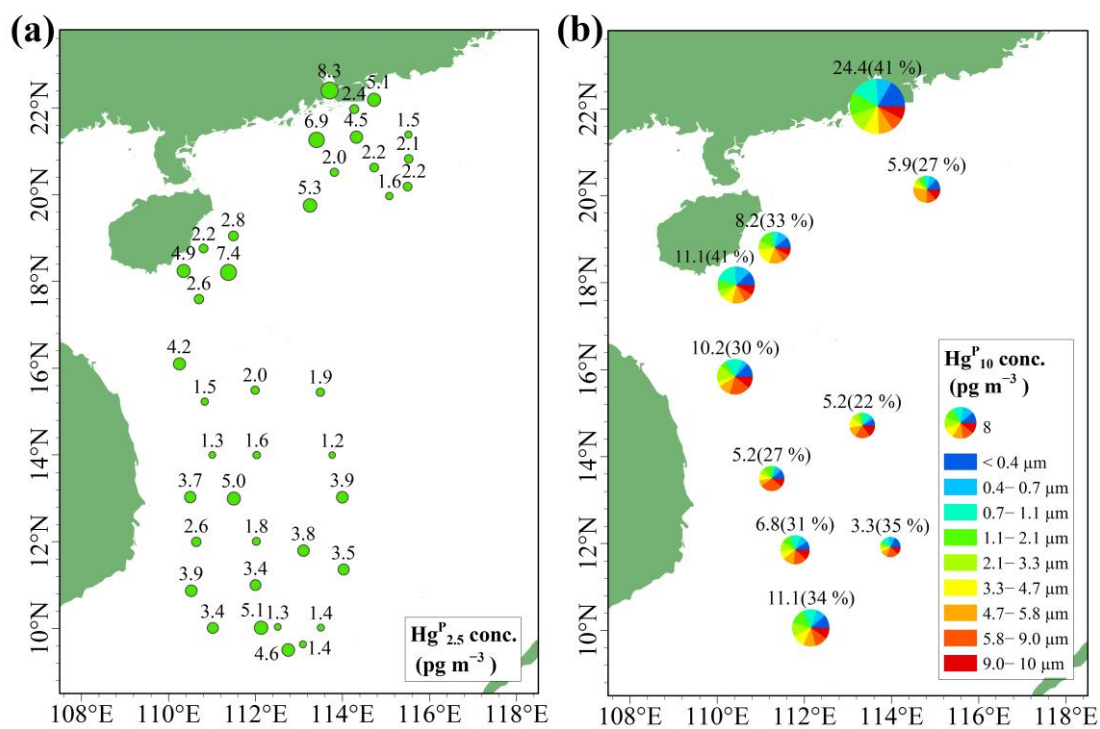
763

764 **Figure 2.** Time (local time) series of GEM, Hg<sub>2.5</sub><sup>P</sup>, RGM and some meteorological parameters,  
 765 including relative humidity (RH), air temperature and wind speed (“A” represents the data  
 766 measured in the PRE, “B” represents the data measured in the northern SCS, “C” represents the  
 767 data obtained in the port of Sanya, “D” represents the data measured in the western SCS). It was  
 768 rainy day on the days of 8 and 26 September 2015.



769

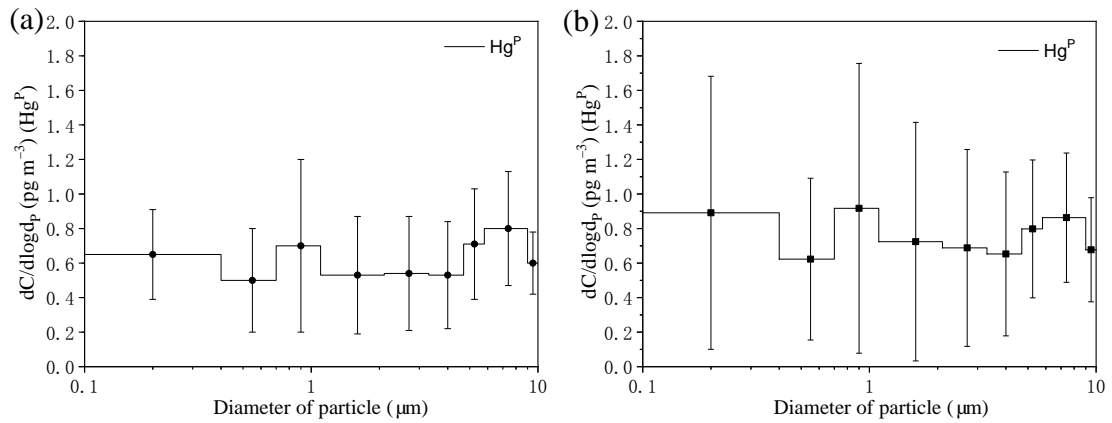
770 **Figure 3.** The concentrations and spatial distributions of GEM (a) and RGM (b) in the MBL of the  
 771 SCS.



772

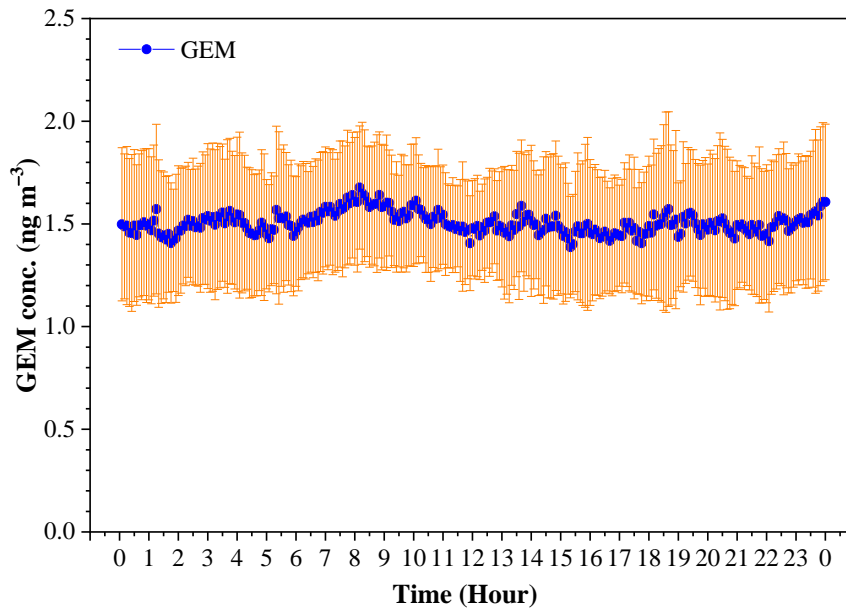
773 **Figure 4.** Spatial distributions of  $\text{Hg}^{\text{P}}_{2.5}$  (a) and  $\text{Hg}^{\text{P}}_{10}$  ( $\text{Hg}^{\text{P}}_{2.1}/\text{Hg}^{\text{P}}_{10}$  ratio) (b) in the MBL of the  
 774 SCS.  $\text{Hg}^{\text{P}}_{2.5}$ ,  $\text{Hg}^{\text{P}}_{2.1}$  and  $\text{Hg}^{\text{P}}_{10}$  denote the  $\text{Hg}^{\text{P}}$  in  $\text{PM}_{2.5}$ ,  $\text{PM}_{2.1}$  and  $\text{PM}_{10}$ , respectively.





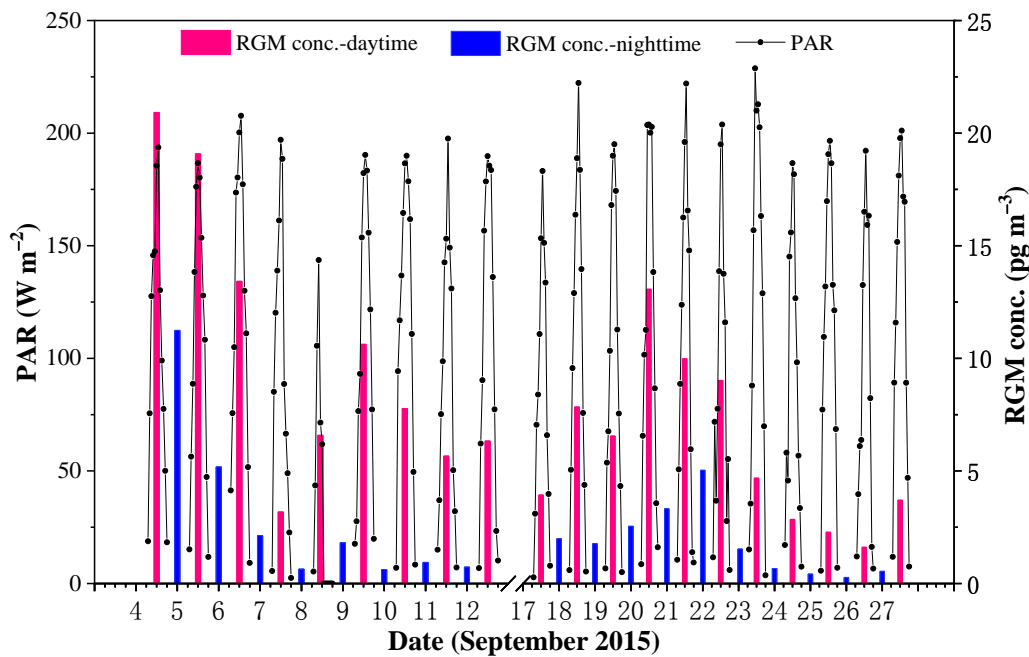
775

776 **Figure 5.** Size distributed concentrations of  $\text{Hg}^{\text{P}}$  (PM<sub>10</sub>) in the MBL of the SCS, (a) represents all  
 777 the data excepting the measurements in the PRE; (b) represents all the data. The data shown are  
 778 the mean and standard error.



779

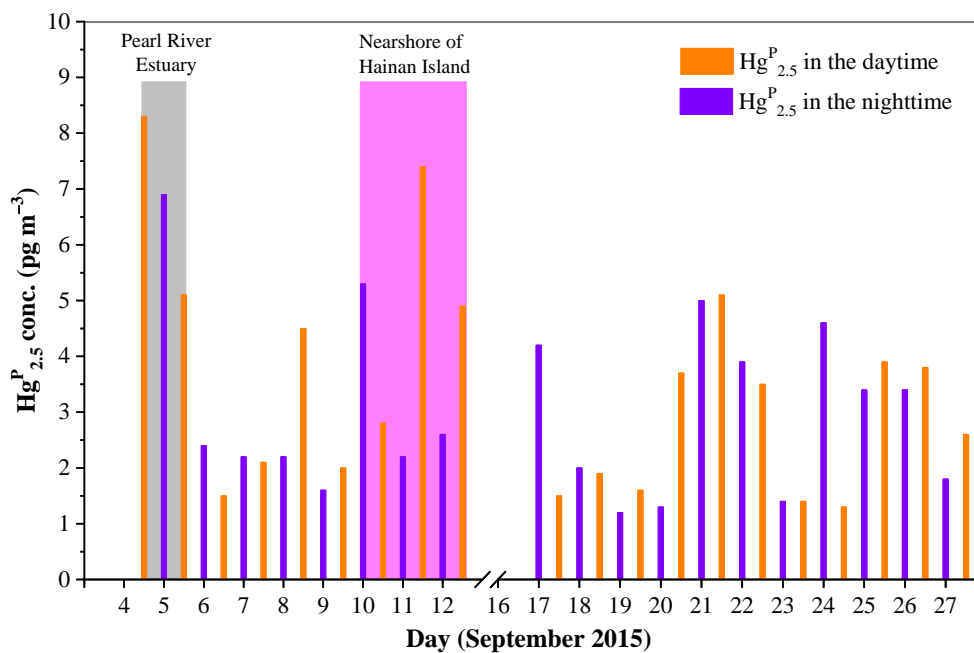
780 **Figure 6.** Diurnal variation of GEM concentration (mean  $\pm$  SD) over the SCS.



781

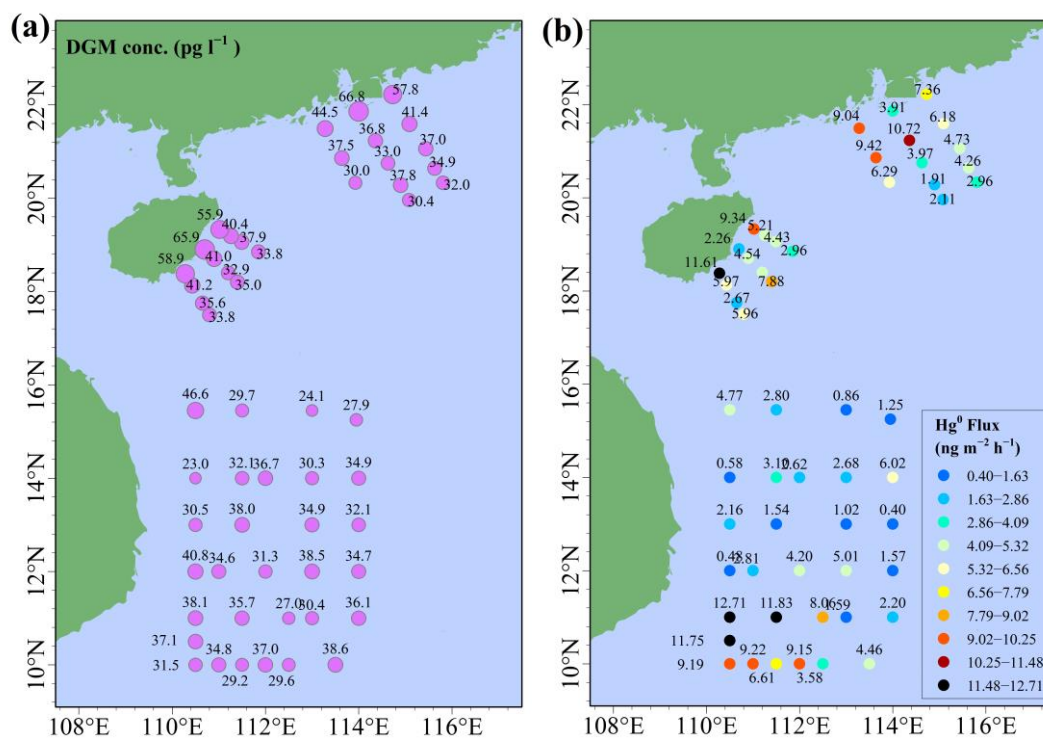
782 **Figure 7.** Daily variation of RGM concentration over the SCS.

783



784

785 **Figure 8.** Daily variation of  $\text{Hg}^{\text{P}}_{2.5}$  in the MBL of the SCS. The light gray area represents the data  
 786 in the PRE, while the light magenta area represents the data in the nearshore area of the Hainan  
 787 Island.



788

789 **Figure 9.** DGM concentrations (a) and sea-air exchange flux of  $\text{Hg}^0$  (b) in the SCS.

790 **Table 1.** The GEM,  $\text{Hg}_{2.5}^{\text{P}}$  and RGM concentrations in this study and other literature.

Location	Classification	Sampling time	GEM ( $\text{ng m}^{-3}$ )	$\text{Hg}_{2.5}^{\text{P}}$ ( $\text{pg m}^{-3}$ )	RGM ( $\text{pg m}^{-3}$ )	Reference	
China	SCS	Sea	2015	$1.52 \pm 0.32$	$3.2 \pm 1.8$	$6.1 \pm 5.8$	This study
	BS and YS	Sea	2014 (Spring)	$2.03 \pm 0.72$	$11.3 \pm 18.5$	$2.5 \pm 1.7$	Wang et al., 2016a, b
	BS and YS	Sea	2014 (Fall)	$2.09 \pm 1.58$	$9.0 \pm 9.0$	$4.3 \pm 2.5$	Wang et al., 2016a, b
	YS	Sea	2010 (Summer)	$2.61 \pm 0.50$	NA <sup>a</sup>	NA	Ci et al., 2011
	YS	Sea	2012 (Spring)	$1.86 \pm 0.40$	NA	NA	Ci et al., 2015
	YS	Sea	2012 (Fall)	$1.84 \pm 0.50$	NA	NA	Ci et al., 2015
	ECS	Sea	2013 (Summer)	$1.61 \pm 0.32$	NA	NA	Wang et al., 2016c
	ECS	Sea	2013 (Fall)	$2.20 \pm 0.58$	NA	NA	Wang et al., 2016c
	Northern SCS	Sea	2007	$2.62 \pm 1.13$	NA	NA	Fu et al., 2010
	Northern SCS	Sea	2003–2005	2.8–5.7	NA	NA	Tseng et al., 2012
	Nam Co	lake	2014–2015	$0.95 \pm 0.37$	$0.85 \pm 2.91$	$49.0 \pm 60.3$	de Foy et al., 2016
	Xiamen	Coastal urban	2012–2013	3.50	61.05	174.41	Xu et al., 2015
Japan	Okinawa Island	Ocean	2004	$2.04 \pm 0.38$	$3.0 \pm 2.5$	$4.5 \pm 5.4$	Chand et al., 2008
Korea	Seoul	Urban	2005–2006	$3.22 \pm 2.10$	$23.9 \pm 19.6$	$27.2 \pm 19.3$	Kim et al., 2009
USA	Weeks Bay	Coast	2005–2006	$1.6 \pm 0.3$	$2.7 \pm 3.4$	$4.0 \pm 7.5$	Engle et al., 2008
Canada	Ontario Lake	Remote area	2005–2006	$1.57 \pm 0.22$	$4.42 \pm 3.67$	$0.99 \pm 1.89$	Cheng et al., 2012
	Nova Scotia	Coast	2010–2011	$1.67 \pm 1.01$	$2.32 \pm 3.09$	$2.07 \pm 3.35$	Cheng et al., 2013
	Nova Scotia	Coast-rural	2010–2011	$1.38 \pm 0.20$	$3.5 \pm 4.5$	$0.4 \pm 1.0$	Cheng et al., 2014
Australia	ATARS <sup>b</sup>	Coast	2014–2015	$0.95 \pm 0.12$	NA	NA	Howard et al., 2017
South-west India Ocean	Ocean	2007	$1.24 \pm 0.06$	NA	NA	Witt et al., 2010	
North Atlantic Ocean	Ocean	2003	$1.63 \pm 0.08$	NA	$5.9 \pm 4.9$	Laurier et al., 2007	
West Atlantic Ocean	Ocean	2008–2010	1.4–1.5	NA	NA	Soerensen et al., 2013	
North Pacific Ocean	Ocean	2002	2.5	NA	9.5	Laurier et al., 2003	
Pacific Ocean	Ocean	2011	1.15–1.32	NA	NA	Soerensen et al., 2014	
Mediterranean Sea	Sea	2000	$1.9 \pm 1.0$	NA	7.9	Sprovieri et al., 2003	
Global Ocean	Ocean	2006–2007	$1.53 \pm 0.58$	NA	$3.1 \pm 11.0$	Soerensen et al., 2010a	
Adriatic Sea	Ocean	2004	$1.6 \pm 0.4$	$4.5 \pm 8.0$	$6.7 \pm 11.7$	Sprovieri and Pirrone, 2008	
Amsterdam Island	Ocean	2012–2013	$1.03 \pm 0.08$	0.67	0.34	Angot et al., 2014	

791

<sup>a</sup> NA: No data available.

792

<sup>b</sup> ATARS: Australian Tropical Atmospheric Research Station.

793 **Table 2.** Correlation coefficients for speciated atmospheric Hg and meteorological parameters (one asterisk  
 794 denotes significant correlation in  $p < 0.05$ , double asterisks denotes significant correlation in  $p < 0.01$ ).

Speciation	GEM		RGM		Hg <sup>P</sup> <sub>2.5</sub>		Wind speed		Air temperature		RH		PAR	
	<i>p</i>	<i>r</i>	<i>p</i>	<i>r</i>	<i>p</i>	<i>r</i>	<i>p</i>	<i>r</i>	<i>p</i>	<i>r</i>	<i>p</i>	<i>r</i>	<i>p</i>	<i>r</i>
RGM	0.069	0.294			< 0.01	0.453**	0.123	-0.251	0.053	0.313	0.065	-0.299	< 0.01	0.638**
Hg <sup>P</sup> <sub>2.5</sub>	< 0.01	0.539**	< 0.01	0.453**			0.037	-0.335*	0.621	0.082	0.434	-0.129	0.432	0.130

795